IEEE Access
Multidisciplinary | Rapid Review | Open Access Journal

Received 20 July 2024, accepted 12 August 2024, date of publication 19 August 2024, date of current version 27 August 2024.

Digital Object Identifier 10.1109/ACCESS.2024.3445371

SURVEY

Segmentation of Overlapping Cells in Cervical Cytology Images: A Survey

E CHEN[1], HUA-NONG TING[1,2], JOON HUANG CHUAH[3,4], (Senior Member, IEEE), AND JUN ZHAO[5], (Member, IEEE)

[1]Department of Biomedical Engineering, Faculty of Engineering, Universiti Malaya, Kuala Lumpur 50603, Malaysia
[2]Faculty of Medical Engineering, Jining Medical University, Jining, Shandong 272067, China
[3]Department of Electrical Engineering, Faculty of Engineering, Universiti Malaya, Kuala Lumpur 50603, Malaysia
[4]Faculty of Engineering and Information Technology, Southern University College, Skudai, Johor 81300, Malaysia
[5]School of Biomedical Engineering, Shanghai Jiao Tong University, Shanghai 200030, China

Corresponding author: Hua-Nong Ting (tinghn@um.edu.my)

ABSTRACT Pap smear testing is crucial for early diagnosis of cervical cancer, but cell overlapping poses a significant challenge to diagnostic accuracy, as improper processing of overlapping cells can lead to misclassification. While significant research efforts have been devoted to segmenting overlapping cells, there is an absence of thorough reviews covering existing studies. This survey represents the first comprehensive exploration of technologies aiming to segment overlapping cells in cervical cytology images. Initially, we collected over 100 relevant papers from various open-source databases using diverse keywords. Subsequently, we conducted a thorough analysis covering various aspects, including datasets, evaluation methods, and data augmentation techniques. We then categorized the applications into conventional machine learning and deep learning approaches, further subdividing both methods into three groups. We summarized articles that utilized conventional machine learning methods and compared the outcomes with those employing deep learning methods. Finally, we provide insights into current challenges and prospects in this critical domain.

INDEX TERMS Cervical cells, overlapping, segmentation, machine learning, survey.

I. INTRODUCTION

Cervical cancer is the fourth most prevalent cancer among women worldwide, with around 604,000 new cases diagnosed in 2020 [1]. As cervical cancer advances, symptoms such as abnormal vaginal bleeding, discharge, and discomfort in the pelvic area may manifest. In its early stages, the disease may not exhibit any signs or symptoms [2]. Cancer progression is not an abrupt process, the progression from benign stages to severe phases usually spans more than 5 years [3]. This disease is entirely preventable and curable when precancerous lesions are identified and treated in time, thereby reducing the occurrence and mortality of cervical cancer [4]. Pap smear was first introduced in the late 1920s and has been extensively used in the early-stage diagnosis of cervical cancer and other related diseases [5], [6]. The traditional Pap smear testing collects cervical cells then stained with hematoxylin to reveal the general morphological characteristics of lesions [7], [8]. Subsequently, the sample was examined by the Pathologists under an optical microscope to identify the degree of abnormalities [9]. A smear, comprising over 5000 cells, often displays various distortions including uneven dyeing, artifacts, overlapping cells, mucus, and blood [10]. The process of analyzing such smears is time-consuming, labor-intensive and subjective, and heavily relies on specialized expertise [11]. As artificial intelligence advances, machine learning (ML) has become more prevalent in automating the identification of cervical cells. Both conventional ML and deep learning (DL) methods used for segmenting and classifying individual cervical cells have shown promising accuracy, comparable to that of human experts [12], [13], [14], [15], [16], [17], [18], [19].

However, during the preparation process of Pap smears, cells tend to cluster together, and cervical cells on the slide are stacked in multiple layers. Cells from upper layers may partially obscure those underneath, indicating that cells in

The associate editor coordinating the review of this manuscript and approving it for publication was Vishal Srivastava.

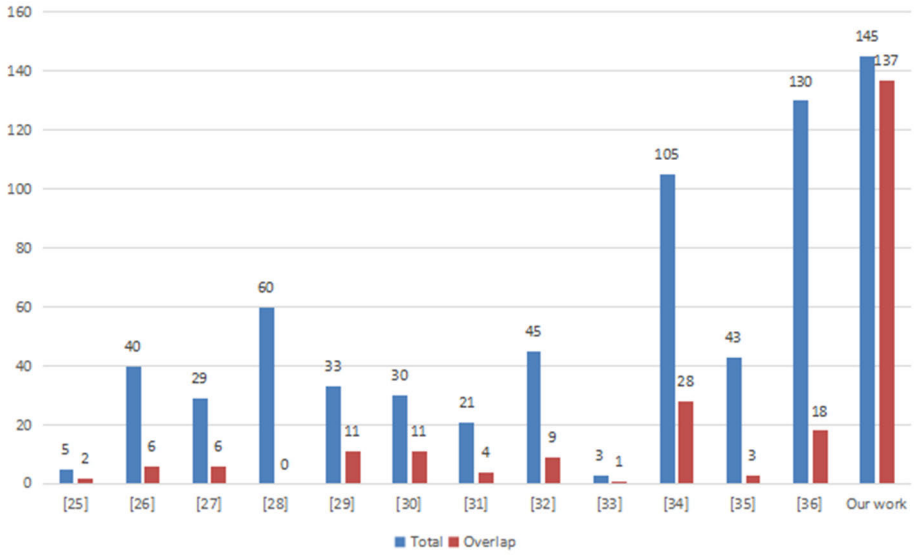

FIGURE 1. Survey comparisons regarding overlapping cell segmentation.

cervical cytology images often overlap and cannot be effectively used for classification [20], [21]. Even Herlev, the manual cropping single-cell dataset for classification task, contains overlapping regions [22]. The large amount of overlapping regions increases the complexity of the cell segmentation. Moreover, classification tasks based on cervical cytology images without proper segmentation of overlapping cells are not feasible, since overlapping cells and malignant cells both can exhibit abnormal shapes and textures, posing a risk of false positive result [23]. Neglecting overlapping cells could consequently lead to false negatives result, impacting the accuracy of diagnosis. While DL-based classification methods may not require precise segmentation of cervical cell contours, segmenting cervical cell regions remains a foundational step for cell analysis. Therefore, precise segmentation of overlapping cells presents significant potential for enhancing the accuracy of cervical cell classification, subsequently enhancing the efficiency of diagnosing and treating cervical cancer.

The initial endeavor to detect overlapping nuclei from cervical cytology images was introduced in 1981 by Bengtsson et al. [24], utilizing the smoothed difference code. Despite this pioneering work, the progress in this area has been hampered by various factors, including privacy constraints on image acquisition, the requirement for specialized expertise and tools for data annotation, and the incomplete development of segmentation algorithms. This landscape changed with the organization of ISBI challenges and the first open-source dataset was released in 2014. Consequently, more researchers began to focus on this field, resulting in a proliferation of studies in cluster cervical cells segmentation. Considering these advancements, there is a conspicuous absence of literature specifically addressing the segmentation of overlapping cervical cells since existing reviews on precancerous lesion detection based on Pap smears focus on single cell segmentation and classification. To provide a clear overview, we conducted a thorough examination of existing survey literature and generated a histogram (Figure 1). Highlighting the number of articles dedicated to the analysis of overlapping cells in the context of cervical cancer analysis. This histogram serves as a comparative tool to illustrate the contributions of each surveyed paper, highlighting the need for our proposed studies in this underexplored area.

This review aims to offer a comprehensive investigation of the existing technologies in automated segmentation of overlapped cervical cells based on Pap smear images. To prepare this review, we conducted searches across various databases, including Google Scholar, PubMed, arXiv, IEEE, Springer and Elsevier. The retrieval terms included ''Pap smear'', ''cervical cytology'', ''overlap'', ''deep learning'', ''segmentation'' and ''cervical cancer''. We excluded studies primarily focused on segmentation without analyzing overlapping cervical cells, even if they claim effectiveness for overlapping conditions, alongside non-English research articles. Additionally, we scrutinized the references and citations within all selected papers. The selected papers encompass various methods, incorporating both conventional machine learning and deep learning approaches. After assessing the full-text articles, over 100 were included in this review, with yearly distribution depicted in Figure 2.

This paper is organized into five sections. Section I provides an overview of the background and objectives of the survey. Section II introduces open-source datasets and evaluation metrics. In Section III, a comprehensive review of cluster

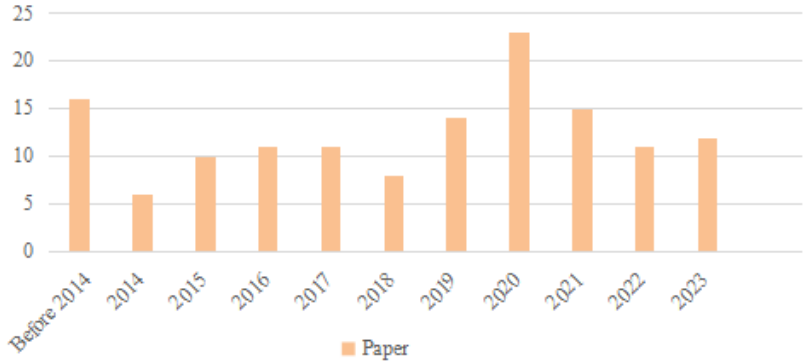

FIGURE 2. Number of studies in overlapping cervical cells segmentation in recent years.

TABLE 1. Summary of open-source datasets.

Dataset	Instances	Task	Link
ISBI2014	645 cells	Cells	https://github.com/luzhi/cellsegmentation_TIP2015
ISBI2015	945 cells	Cells (training and testing)	http://goo.gl/KcpLrQ
Cervix93 (2018)	2705 nucleus	Nucleus	https://github.com/parham-ap/cytology_dataset
BTTFA (2019)	104 images	Nucleus	https://data.mendeley.com/datasets/jks43dkjj7/1
Cx22 (2022)	1320 images (7473 cells)	Cells (training and testing)	https://github.com/LGQ330/Cx22
CNSeg (2023)	124,353 nuclei	Nucleus (training and testing)	https://www.kaggle.com/datasets/zhaojing0522/cervical-nucleus-segmentation

cervical cell analysis is presented, covering both ML and DL approaches. Section IV discusses challenges, future directions, and insights in this field. Finally, Section V concludes this work.

II. DATASETS AND EVALUATION METHODS

In this section, we summarize the open-source datasets used in overlapping segmentation tasks, as outlined in Table 1. We excluded the Herlev and SIPaKMeD datasets from our study. While they are utilized in certain research for tasks such as overlapping fragment segmentation and boundary detection, they lack multiple whole cells in a single image. Our focus is primarily on segmentation tasks; hence we chose to overlook datasets that provide only class labels without boundary annotations. The description of the open-source dataset is presented in Table 1, and a single image retrieved from the open-source dataset is shown in Figure 3.

ISBI 2014 [37], the first open-source dataset for the Overlapping Cervical Cytology Image Segmentation Challenge, was released by the IEEE International Symposium on Biomedical Imaging. The dataset comprises 16 non-overlapping fields of view images at 40× magnification, containing 645 cells with boundary annotations for cytoplasm and nucleus. The image resolution is approximately 0.185 μm/pixel.

ISBI 2015 [38]. This dataset was released in 2015 for the second cervical cell segmentation challenge. The ISBI 2015 expanded from ISBI 2014 to include 945 images through a synthesis process, which involved manually annotating the cytoplasm of 13 isolated cervical cells. images in ISBI 2015 exhibit a range of cell counts, spanning from 2 to 10, and overlapping coefficients ranging from 0 to 0.5.

Cervix93 includes 93 stacks of images at 40× magnification, each stack containing between 10 and 20 images acquired from evenly distributed field views spanning from the slide's top to bottom, with manually marked internal points and boundary information of nuclei. [39]. This dataset includes varying levels of cell overlap, with 2705 nuclei annotated via bounding boxes.

Dataset used in BTTFA [40], An LBC-based dataset comprises 104 images, each sized at 1024 × 768, with nucleus boundary labels assigned to every image by professional pathologists. Compared to conventional Pap smear, LBC requires an additional sample treatment process to remove impurities. As a result, LBC offers superior image quality but also comes at a higher cost.

The CCEDD dataset, introduced by Liu et al. [41] comprises 686 cervical images, each sized in 2048 × 1536 pixels. Optical magnifications of 100× are applied for patients with

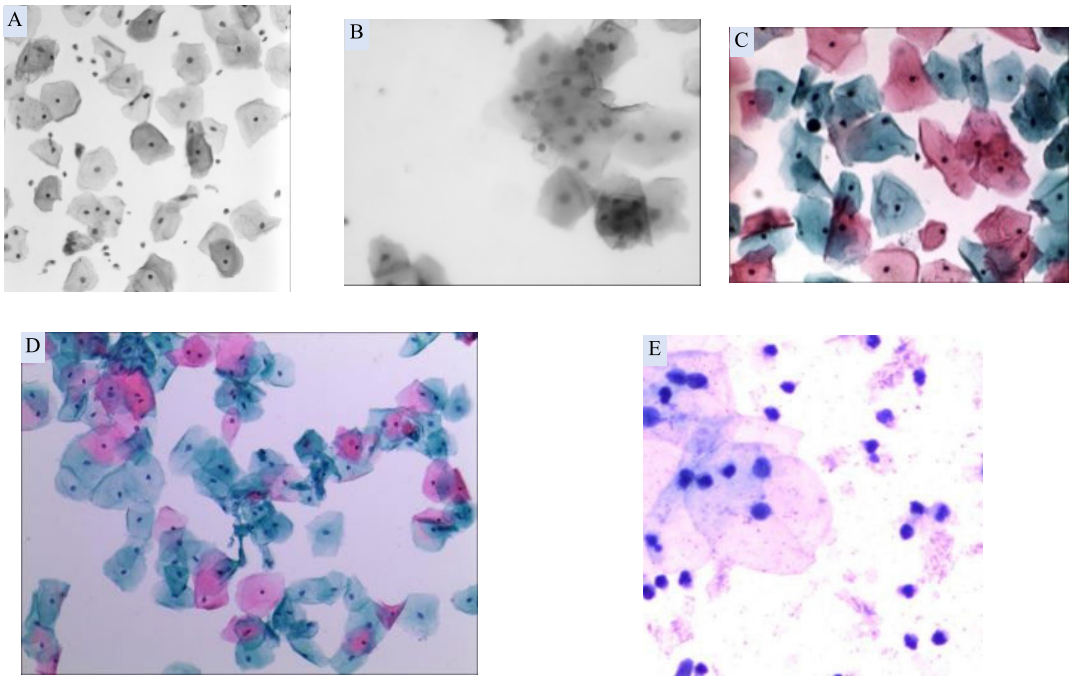

FIGURE 3. Image from A. ISBI, B. Cervix93, C. BTTFA, D. Cx22, E. CNSeg.

negative cervical cancer, and 400× for those with positive cervical cancer. The cytoplasm and nucleus boundaries in this dataset were annotated by six expert cytologists, with each CCEDD image containing only a label for the cell edges, making it unsuitable for instance segmentation due to the lack of specific object labels. In contrast, Cx22 is based on the CCEDD. Zhao et al. [42] manually delineated the contours of 7473 instances of nucleus and cytoplasm across 1320 images, cropping the original images to 512 × 512 pixels. Cx22 includes two subsets: Cx22-Multi and Cx22-Pair. In Cx22-Pair, images consist of two overlapping cervical cells, while Cx22-Multi comprises training (Cx22-Multi-Train) and testing (Cx22-Multi-Test) datasets.

The CNSeg dataset comprises 1530 samples scanned at 40× magnification [43]. The dataset uses LabelMe to delineate the boundaries of the nuclei. The CNSeg dataset consists of three subsets: the PatchSeg, which includes 85882 nuclei in 3487 images with a size of 512 × 512; the ClusterSeg, which includes 34,311 nuclei in 2361 images with overlapping nuclei; and the DomainSeg dataset, which comprises two different staining method datasets. TargetA includes 381 images, with 145 images labeled for testing, while TargetB consists of 332 images, with 57 images labeled for testing.

In the domain of segmentation tasks, the primary evaluation metrics operate at the pixel level. Foremost among these is the Dice coefficient (DC), followed by precision (Prec), sensitivity (Sens), and recall (Rec), These metrics are primarily used to evaluate the effectiveness of conventional machine learning methods. These metrics are also applicable for evaluating the segmentation performance of deep learning methods. Additionally, other evaluation metrics include the average Jaccard index (AJI), panoptic quality (PQ), Hausdorff distance (HD), F1 score, intersection over union (IoU), and Zijdenbos similarity index (ZSI).

Object-wise evaluation metrics, such as False Negative Rate (FNRo), are comparatively less prevalent but still relevant. Overall, the formulas for these metrics are adapted to suit segmentation tasks, with the IoU and Jaccard Index (JAC) formulas being interchangeable, and the F1 formula being equivalent to DC. All the metrics are listed in Table 2.

III. IMPLEMENTATIONS

In this section, we summarize literature regarding various ML and DL models in the overlapping cervical cells separation. Conventional machine learning methods rely on handcrafted feature extraction guided by prior knowledge. This process typically involves preprocessing, coarse segmentation, fine segmentation, and data enhancement techniques like smoothing and denoising. In contrast, deep learning methods utilize multi-layered architectures and millions of parameters. They use data augmentation techniques including rotation and flipping. Additionally, pre-trained models are frequently employed in deep learning applications. Additionally, we summarize the performance of deep learning models in segmenting the overlapping cells.

A. DATA ENHANCEMENT

1) QUALITY ENHANCEMENT

Pap smear images commonly contain impurities during staining. Additionally, limitations in imaging techniques may result in out-of-focus, low-resolution and poor contrast in

TABLE 2. Summary of evaluation metrics.

Metric	Definition	Description
TP/TN/FP/FN	True Positive, True Negative, False Positive, False Negative.	TP: Positives predicted correctly. TN: Negatives predicted correctly. FP: Predicted positives as false. FN: Predicted negatives as positives.
Pixel-wise and Object-wise		
Precision (Prec)	$\frac{TP}{TP+FP}$	The proportion of accurately predicted positive among all predicted positives.
Recall (Rec)	$\frac{TP}{TP+FN}$	The proportion of predicted positive instances to the total true positive.
Accuracy (Acc)	$\frac{\mathrm{TP}+\mathrm{TN}}{\mathrm{TP}+\mathrm{TN}+\mathrm{FP}+\mathrm{FN}}$	The ratio of correctly predicted to the total number of samples.
Specificity (Spec)	$\frac{TN}{TN+FP}$	The ratio of samples accurately predicted as negative among all negative samples.
Sensitivity (Sens)	$\frac{TP}{TP+FN}$	The ratio of accurately predicted positive among the total positive cases.
Pixel-wise		
F1	$\frac{2*Prec*Rec}{Prec+Rec}$	This metric, ranging from 0 to 1, considers both Precision and Recall, with values closer to 1 indicating superior model performance.
Dice Similarity coefficient (DC/Dice/DSC)	$\frac{2*TP}{FP+FN+2TP}$	The value ranges from 0 to 1, with higher values indicating better overlap between predicted and true regions.
IOU	$\frac{TP}{TP+FN+FP}$	The intersection over union(IOU) between the predicted and ground truth regions.
Hausdorff distance	$\max\{D(i): S_i \neq R_i\}$	The Hausdorff distance is the maximum among the set of shortest distances between two shapes.
Zijdenbos similarity index (ZSI)	DC	ZSI employs the same formulation as DC.
Jaccard Index (Jac)	IOU	Jac employs the same formulation as IOU.
Average Jaccard Index (AJI)	$\frac{1}{N}\sum_{i-1}^{N}\frac{TP_i}{TP_i+FN_i+FP_I}$	Average of the Jaccard Index of all instances.
Panoptic Quality (PQ)	$\frac{\sum_{(P,g)\in TP} IOU_{(p,g)}}{\lvert TP\rvert+\frac{1}{2}\lvert FP\rvert+\frac{1}{2}\lvert FN\rvert}$	The average intersection over union (IoU) of all correctly matched pairs of pixels
AP	$\frac{\sum_{k=1}^{n} P(k)\times Rec(K)}{N}$	The average precision across the precision-recall curve.
Object-wise		
FNRo	$\frac{FN_o}{TP_o+FN_o}$	False negative rate at object level. If a DC is below a certain threshold (typically 0.7), it is considered an undetected object.

cervical cytology image. Image preprocessing techniques such as median filtering, guided filter, histogram normalization, histogram equalization, contrast enhancement and edge sharpening was applied to improve the image quality [44]. Malm et al. [45] applied a multi-step approach based on the area, shape, texture and intensity to remove the debris. Advanced techniques, such as contrast local adaptive histogram equalization (CLAHE) and integration with the Diffusion-Stop-Function, were employed to enhance contrast and eliminate noise [46]. Conversely, Gaussian noise and salt pepper noise were introduced to enhance generalization [47]. Furthermore, a gradient decomposition method was applied to enhance edges and suppress artifacts in the images [48]. Kaur and Sahambi [49] proposed a multiscale top-hat transform and h-maxima to enhance in images with very low contrast and where cells are touching.

The common use of the RGB color space in image analysis poses challenges in addressing issues such as poor contrast and uneven illumination during slide acquisition. This has prompted a preference for the CIE L*a*b* color space, renowned for its superior capabilities in managing brightness and representing a wide range of colors. Since the L* channel represents the brightness level and a* channel represents variations between red and green, researchers

employed the a* channel for background extraction [50], [51]. Zhang et al. [52] transformed the original images to grayscale by extracting the V channel value from the HSV color space to enhance the contrast.

2) QUANTITY ENHANCEMENT

Data augmentation has been proven to be an effective solution for overcoming the challenge of limited datasets and insufficient diversity when using DL models. Traditional data augmentation methods include inversion, rotation at multiple angles, flipping, and scaling were employed to enrich image diversity, leading to a significant improvement in accuracy and robustness [53]. Cervical cells are typically distributed across multiple focal planes. Researchers initially capture images containing single cells from various focal planes, manually delineate them to establish the ground truth, and subsequently convert these delineated images into a single extended depth of field (EDF) image. Lu et al. [38] constructed 945 synthetic overlapping images from single EDF cervical cell images, i.e., ISBI 2015. Umadi et al. [54] obtain an additional 280 images for training based on the same EDF image. Researchers also applied the Beer-Lambert Law to reconstruct the pixels of the overlapping parts. Mahyari et al. [55], [56] generated 5000 and 100,000 new overlapped images from the ISBI 2014 dataset. Generative Adversarial Network (GAN) were also applied for image synthesis, Geng et al. [57] applied conditional GANs, combining U-Net, DenseBlock and semantic segmentation network to generate 5000 blurred images from single-focus and few-focus images.

B. CONVENTIONAL MACHINE LEARNING

We categorize conventional machine learning approaches employed for segmenting overlapping cervical cells into the following categories: region-based methods, pixel intensity methods, and contour methods.

1) REGION-BASED METHODS

Region-based segmentation methods partition an image into distinct areas based on criteria such as color, texture, or intensity, allowing for deeper analysis and understanding of image content. Commonly utilized approaches in this category include superpixel, region growing, watershed, Voronoi and Graph cut. Description and results of region-based segmentation methods are presented in Table 3 and Figure 4.

The Superpixel algorithm, renowned for its ability to divide pixels into perceptually meaningful atomic regions based on similar sizes, intensity, texture and distance, provides a robust method to reduce complexity and improve computational efficiency. This pre-segmentation method is particularly promising for handling low-contrast images. Yet, improper selection of hyperparameters, such as superpixel size and color space distance measurement can result in either over-segmentation or under-segmentation. The Simple Linear Iterative Clustering (SLIC) is designed for superpixel generation [58]. Initially, the algorithm transfers the original image to the CIE-Lab color space, creating a five-dimensional vector $V[L, a, b, x, y]$ for each pixel, comprising (L, a, b) color values and (x, y) coordinates. Then, k seed points are randomly initialized, and neighboring pixels with similar vectors are iteratively grouped until all pixels are classified. Subsequently, the algorithm recalculates cluster centers and performs clustering until convergence. Notably, SLIC ensures boundary continuity by constraining the search region to a size proportionate to the superpixel size, achieving linear complexity with respect to pixel count and independence from superpixel quantity. Tareef et al. [59] employed the SLIC algorithm to produce an over-segmented superpixel map, dividing the image into locally coherent clusters with homogeneous regions. Lee and Kim [60] utilized the SLIC method to generate over-segmented superpixels. Subsequently, mean intensity values are calculated for each region to create the mean-value image for extracting cellular clumps. Diniz et al. [61] utilized the SLIC algorithm to detect nucleus candidates by partitioning the original image into regions with approximately equal sizes, consistent intensity, and pixel distance.

Mean Shift, a non-parametric density estimation method employed for generating superpixels was proposed by Comaniciu and Meer [86]. It involves iteratively shifting data points in feature space towards the direction of maximum local density until convergence to the peak of the density estimate, followed by clustering of the data. Zhang et al. [74] applied mean shift to partition the cells into different color segments. Quick Shift generates superpixels through a mode-seeking segmentation approach [87]. It begins segmentation via a medoid shift procedure. where point in the feature space is then shifted to its nearest neighbor, aiming to converge towards the peak of the density estimate. Harangi et al. [66] employed the quick shift to delineate the boundaries among nuclei and cytoplasm. Khadidos et al. [68] employed the quick shift to segment the EDF image into regions representing cells and background. The output is a superpixel map consisting of regions assigned values in the range [0,1].

Region growing segment the image by connecting pixels with similar characteristics and iteratively grouped together to form regions, based on predefined criteria such as intensity, color, or texture similarity. While effective, this method is sensitive to initial seed selection, incorrect seeds may lead to over-segmentation or under-segmentation. Sulaiman et al. [79] applied preselected pixels as initial seed points and set preselected minimum values as threshold values for cytoplasm and nucleus pixels. These seed pixels were expanded to neighboring pixels, incorporating them into the region until their pixel values were less than or equal to the preselected threshold.

The Watershed algorithm, inspired by geographical "watersheds," interprets the image as a topological surface, with pixel values resembling heights. It identifies regional minimal values as catchment basins and maximal values

TABLE 3. Description of region-based methods.

Method	Advantage and limitation	References
Superpixel	A pre-processing step used to reduce computational complexity. Easy to over-segmentation or under-segmentation	[59],[60],[61],[62],[63],[64],[65],[66],[67],[68],[69],[70],[71],[72],[73],[74],[75],[76],[77]
Region growing	Flexibility and robustness to noise. Sensitive to seed and parameters.	[78],[79],[80]
Watershed	Efficient for weak boundaries and low contrast. Under-segmentation and sensitivity to noise.	[50],[73],[74],[75],[81],[82], [83]
Voronoi	Computational efficiency, Generality and universality. Results in polygons or polygon-like shapes.	[67],[73],[74],[77],[84],[85]
Graph cut	Utilizes both boundary and regional information, without any prior knowledge. Slow with high resolutions image	[51],[76]

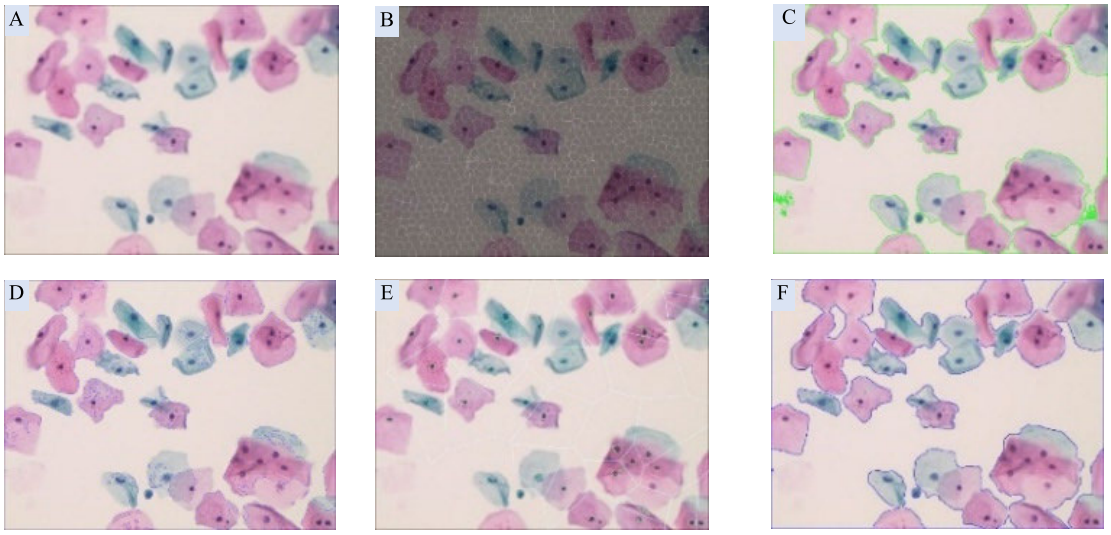

FIGURE 4. A. original image, B. Superpixel, C. Region growing, D. Watershed, E. Voronoi and F. Graph cut.

between neighboring basins as ridge lines. The goal of watershed-based segmentation is to detect these ridge lines within the image. This method is commonly applied to the gradient image, where objects correspond to basins and boundaries to ridges. Zhang et al. [74] utilized the watershed algorithm to split superpixels and filter nuclei based on their eccentricity, average gray value, and area size. Tareef et al. [75] introduced a Multi-Pass Fast Watershed (MPFW) method for automatic separation of nucleus and cytoplasm from clustered cells. The first watershed pass integrates intensity gradient details to segment nuclei. The second and third passes are used to segment partially overlapped and highly overlapped cytoplasm. The disadvantage of this method is that noise and local irregularities in the gradient may lead to under-segmentation.

The Voronoi algorithm, named after mathematician Georgy Voronoi, divides a plane into distinct areas based on the closest distance to a specific group of points called seeds or generators. In image segmentation, each pixel is associated with the seed closest to it. This method is sensitive to the distribution of seed points and may result in irregular boundaries, leading to uneven segmentation. Ushizima et al. [67] partitioned the image into convex polygons, ensuring that each Voronoi polygon encompasses one nucleus. Ramalho et al. [73] utilized a combination of the Voronoi diagram and ellipse shape to detect the cytoplasm border. Yang et al. [84] utilized the Voronoi diagram to generate the initial boundary of each cell based on the labeled points.

Graph partitioning treats the image as a graph, with nodes representing pixels and edges illustrating their relationships. The complexity remains unaffected by the number of target objects. By employing the max-flow/min-cut method, t minimizing the energy function to distinguish the cellular from the background. Graph cuts become slower with higher image resolutions due to the increased number of nodes. Typically, Graph Cut is applied to pre-segmented or coarsely segmented results and requires specifying foreground and

TABLE 4. Description of pixel intensity-based methods.

Method	Advantage and limitation	References
Thresholding	Computational efficiency, simplicity and Versatility. Dependency on threshold selection, not suitable for low contrast image.	[52],[59],[60],[62],[65],[68], [71],[78],[79],[80],[82], [83],[84],[89],[90],[91],[92],[93], [94],[95],[96],[97],[98],[99],[100]
Morphological operations	Reduce noise, detect edge, robustness to illumination and contrast variations. Distortion of objects, Introduction of artifacts in complex images.	[64],[65],[72],[100],[101], [102],[103]
Clustering	Flexibility and robustness in various image conditions. Sensitivity to the number of clusters and initial centroids, Vulnerability to local minima.	[23],[48],[71],[80],[90],[99], [104],[105],[106],[107]

background to accurately extract target objects from the background. Zhang et al. [51] proposed global graph cuts for cytoplasm segmentation and local graph cuts for nuclei segmentation. They applied multi-way graph cuts to the image enhanced with the a* channel for cytoplasm segmentation. Additionally, they employed graph cuts combined with intensity, texture, contour, and region information for nuclei segmentation. Song et al. [76] utilized a graph partitioning model to enhance spatial consistency, resulting in accurate delineation of objects based on the superpixel segmentation. Zhang et al. [88] utilized a graph-based random walk model to delineate the cytoplasm contour. This model constructs an edge between two nodes in a 4-connected neighborhood grid, with edge weights computed using a Gaussian function based on the similarity measure between neighboring nodes.

2) PIXEL INTENSITY-BASED METHODS

Pixel intensity-based methods segment images by the brightness or color values of individual pixels to distinguish between different regions or objects. These methods, include thresholding, morphological operations, k-means, and distance transform, assign pixels to specific regions based on their intensity levels. The pixel intensity-based segmentation methods and their corresponding results are detailed in Table 4 and illustrated in Figure 5.

Thresholding methods segment images into distinct regions based on the intensity or value of each pixel. They are among the simplest, easiest, and fastest segmentation methods available. Yet, finding an appropriate threshold that effectively separates the image into two groups is not always straightforward. Moreover, this method relies on the assumption that the foreground and background in the image have significantly different intensity values, which may not always be the case. In scenarios with low image contrast, local thresholding may be preferred over global thresholding to more effectively adapt to varying intensity levels across the image. The Otsu, analyzes the histogram of pixel intensities in the image to identify an optimal threshold to divide the image into foreground and background [108]. This approach relies on the grayscale intensity values of the image, The implementation of a single threshold can effectively segment the cervical cells from the image [89], [90]. Zhang et al. [74] applied a brightness threshold to remove the background using the luminance histogram. Somasundaram et al. [92] proposed a multi-thresholding method to segment the nucleus from the background. This method was inspired by the observation that multiple peaks in the histogram correspond to different objects in the image. Iram Hoque et al. [109] introduced an adaptive thresholding method with seven tunable parameters to enhance nucleus segmentation in cervical images.

Morphological operations are a set of image processing techniques employed for analyzing and processing shapes within images. They involve manipulating morphology (shape and structure) in images through operations like dilation, erosion, opening, and closing. These operations serve to fill holes in the image, connect or separate objects, and excel in tasks such as noise removal, edge detection, and feature extraction. Conversely, they are vulnerable to image noise and may alter the size and shape of objects, risking loss of detail or introduction of artifacts. Additionally, traditional morphological operations utilize a uniform size of the structural element (SE) on all cells, which may produce unwanted outcomes when handling overlapping cells. Afaf Tareef et al. [103] employed morphological filters, including opening and closing operations, to smooth areas with extreme values. This process resulted in flat maxima within the cellular clump. Wang et al. [64] introduced a flexible morphological operation tailored for overlapped cells. They defined the maximum and minimum erosion radius of the structural element based on cytological knowledge and image characteristics. Zhao et al. [101] utilized morphological operations to eliminate false nucleus edges extracted by the Canny operator, which were caused by noise. The process involved applying dilation and erosion to the binarization of the nucleus ROI.

The K-means clustering technique, aims to divide a set of n observations into k clusters. In the context of segmenting cell images, it partitions them into distinct clusters based on pixel intensity or other feature vectors. Each pattern cluster maintains a single center throughout the process. This method iteratively recalculates the centroids to minimize the sum of squares within each cluster. Guven and Cengizler [23] utilized k-means clustering based on two texture features and three shape features to determine the presence or absence of overlapping. In their study, Guan et al. [48] combined morphological filtering with the K-means clustering algorithm

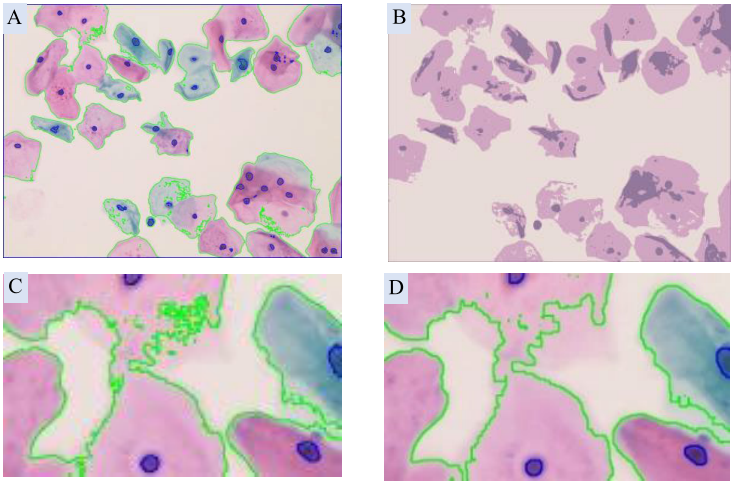

FIGURE 5. Segmentation results, A. 2-thresholding, B. 3-cluster FCM, C and D. 2-thresholding and Morphological operations.

for pre-segmentation. Initially, they employed morphological filtering to mitigate contamination effects. Subsequently, they categorized pixels into four groups—nuclei, dark cytoplasm, light cytoplasm, and background—based on the L* channel of the CIELAB color space using the K-means clustering. Additionally, they merge pixels with median gray levels into a single class representing the cytoplasm. Riana et al. [99] employed the K-means to detect cytoplasm, utilizing color features extracted from the Lab image, which includes the L (luminance), a (red color), and b (blue color) components. Umadi et al. [54] applied a four-cluster K-means algorithm to group pixels by intensity, to create a cell clump mask.

The fuzzy c-means (FCM) clustering, unlike K-means clustering, takes into account the fuzzy relationship between each pixel and each cluster center. In FCM, data points may have memberships in multiple clusters, with degrees ranging from 0 to 1, and the centroids are determined by the weighted average of these memberships. Clustering is achieved through an iterative algorithm that updates cluster centers and coefficients during each iteration. Eventually, all observations are assigned to distinct clusters by the conclusion of the iteration process. Guven and Cengizler [23] employed FCM based on two texture features and three shape features to discern the presence or absence of overlapping. Their approach yielded a higher F1 score and faster processing compared to k-means clustering. Standard FCM typically only considers intensity information and lacks spatial information. Saha et al. [90] utilized FCM in conjunction with a spatial shape function, enabling precise segmentation of nuclei.

The GMM (Gaussian Mixture Model) models data distribution as a linear combination of multiple Gaussian distributions. The EM algorithm trains the GMM by learning the parameters of each component and assigning pixels to the component with the highest probability for segmentation. Jung et al. [107] utilized GMM to segregate overlapping nuclei. This method was also employed to separate cell clusters from background [71], [80].

3) CONTOUR-BASED METHODS

Contour-based methods separate images by detecting and tracing the boundaries of objects or regions of interest. These methods analyze the edges or outlines present in the image to delineate distinct shapes or textures by identifying changes in pixel intensity or gradients. Nevertheless, these methods are sensitive to initialization, as poor starting points can lead to convergence on local minima or struggle in low-intensity regions. Additionally, they may perform poorly when segmenting touching boundaries or blurred edges and can be computationally complex. Table 5 provides an overview of contour-based methods, while Figure 6 showcases the results of edge detection.

An active contour, also known in the field as snake, is a deformable curve within an image that evolves based on both internal and external forces. Internal forces arise from the curve itself, encompassing properties like smoothness and length. Meanwhile, external forces stem from image information, such as edges or object boundaries. This elastic curve starts from an initial position, provided either interactively by the user or through higher-level processes, and moves towards features to extract by minimizing energy. The accuracy of the performance relies on the initial curve placement, necessitating its positioning around the target region for evolution. Plissiti et al. [110] introduced a method akin to ACM, integrating physically based modeling with an active shape model. This approach utilized prior knowledge of the anticipated shape and variable weights in the computation of the image force to achieve accurate segmentation of two overlapping nuclei. Similarly, Araújo et al. [111] employed active contours to segment overlapping cells, demonstrating robustness in handling a vast number of cells and highly overlapped instances.

TABLE 5. Description of contour-based methods.

Methods	Advantage and limitation	References
Active Contours	Boundaries can be easily detected. Minimizing energy is time-consuming.	[48],[68],[110],[111]
Edge Detection	Efficient at detecting object boundaries. Ineffective in cases of ill-defined or excessive edges.	[80],[101],[112],[113],[114]
Level Set	Robustness to intricate image structures and boundaries. Sensitivity to initialization.	[37],[38],[47],[63],[65],[69],[70], [71],[72],[84],[94],[95],[96],[101], [104],[105],[106],[115],[116], [117],[118],[119],[120],[121],[122]
Shape Models	Efficient representation of object shape, robustness to variations in appearance. Limited ability to handle complex shapes.	[47],[66],[69],[76],[77],[84],[85], [103],[107],[119],[123],[124],[125], [126],[127],[128],[129],[130],[131]

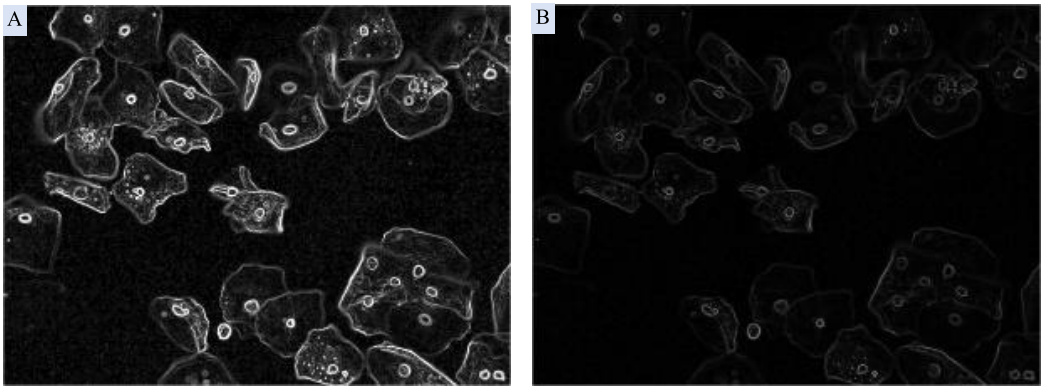

FIGURE 6. A. Scharr edge, B. Sobel edge

Edge detection is crucial in image processing as it reveals discontinuities in physical, photometric, and geometric properties of objects within a scene, providing important visual information. This operation involves extracting object contours while ignoring extraneous details, thereby simplifying image analysis by reducing data volume. There are two main categories of edge detection methods: gradient-based techniques, which utilize first-order derivatives and are relatively simple to implement with lower computational costs but are sensitive to noise. Examples include Sobel, Prewitt, Roberts, and Canny operators. In contrast, Laplacian-based methods employ second-order derivatives to assess the rate of change in image gradients. These methods capture the acceleration of intensity changes, making them suitable for high-precision and complex edge detection tasks. While they are less sensitive to noise, they may struggle with coarse or blurred edges. Kumar et al. [95] converted the image into a binary format to obtain the edges of cell clusters. Tareef et al. [59] utilized the Anisotropic Diffusion Filter (ADF) to eliminate noise and extraneous details while retaining edge information in the image. Plissiti et al. [110] utilized the Canny edge detector on preprocessed images to detect strong boundary edges as the optimal matching position for searching the initial model. Phoulady et al. [80] used a pre-defined similarity metric to detect the approximated boundaries. Researchers have also employed transformers for edge detection in small-scale datasets [132].

The Level Set method, a widely used image segmentation technique, iteratively evolves a contour within the image domain by minimizing an energy functional derived from features like gradients, intensities, or edges. This dynamic adjustment, often constrained by iterations, contour size, length, an ellipsoidal shape prior, and cytoplasm curvature. The performance of the Level Set algorithm is influenced by the placement of seed points or initial contours. This approach involves initially determining the estimated position of the cell cytoplasm and then selecting the surrounding region for evolution. Negar M. Harandi et al. [94] employed an automatic circular decomposition method to generate the initial contour for overlapping cells. Lu et al. [69] utilized constraints based on a single contour area, length, and an assumption of elliptical shape as the initial curve for evolution, and subsequently utilized unary and pairwise constraints for generating the initial curve [37]. Unary constraints were determined by contour area, edge strength, and cell shape, while pairwise constraints were derived from the areas of overlapped regions. Islam and Haque [116] proposed a Multi-step Level Set approach to delineate nuclei and cytoplasm from overlapped cells. This method incorporates parameters including cytoplasm curvature, retention duration of segmented cytoplasm, boundary information, and a pace controller dependent on cell homogeneity. Nisar et al. [96] proposed initializing the Level Set with a circle of radius 20. Tareef et al. [70] utilized cell boundaries as the initial curve

based on the classification result of SLIC. Li et al. [71] utilized a square grid with a fixed width as the initial region. addressed the problem of erroneously detected fragments that resulted from faulty initialization of contour points by applying a signed distance function. Wang et al. [120] obtained seed contour points from a gradient map to generate a rough segmentation contour, which was further improved through Distance Regularized Level Set Evolution (DRLSE).

Shape models, describe object shape features using prior knowledge or sample data. Researchers use statistical-based predefined templates, such as ellipses and star shapes, to match the shapes of the objects in the images. This expected description aids in precise localization and segmentation of cell boundaries. The elliptical shape prior is commonly used in delineating the single-cell boundary in cluster cells [73], [78], [110], [119]. Instead of employing elliptical shapes, Song et al. [47] introduced a dynamic multiple-template deformation model, utilizing multiple cell labels as input. They integrated structural and contextual information to deform cell shapes effectively. Following this, they trained a shape prior model to achieve precise segmentation results. Nosrati and Hamarneh [85] utilized a star-shaped prior rather than elliptical shapes for segmentation. Following the attainment of precise segmentation in polar coordinates, they converted back to Cartesian coordinates to obtain the results. Zhao et al. [133] employed star-convex polygons to estimate and locate cervical cells in Pap smear images. Tareef [127] introduced an Adaptive Shape Prediction Model for overlapped cell segmentation, relying on the cellular cluster boundary. This approach involves deformation based on contours and shapes.

C. DEEP LEARNING

We categorize deep learning methods into semantic segmentation, instance segmentation, and GANs. Semantic segmentation typically employs CNNs and U-Net and requires post-processing to achieve precise cell edges. Instance segmentation commonly utilizes networks such as Mask R-CNN and incorporates enhanced feature extraction modules. GANs employ adversarial approaches for segmenting overlapping cells.

1) SEMANTIC SEGMENTATION

Semantic segmentation categorizes an image into three classes: cytoplasm, cell nuclei, and background, assigning each pixel to one of these categories. This approach does not differentiate between individual cell instances or effectively segment overlapping regions. To address the segmentation of overlapping cells, post-processing methods are employed. These methods are used to refine the boundaries of individual cells within overlapping areas. Harangi et al. [66] applied an ensemble approach combining FCNNs and conventional machine methods to localize cell cluster boundaries at the pixel level. Two variants of FCNNs, namely FCN-8 and FCN-16, were utilized in conjunction with results of the quickshift. Additionally, two consensus methods were employed to integrate the outputs of deep learning and conventional machine methods.

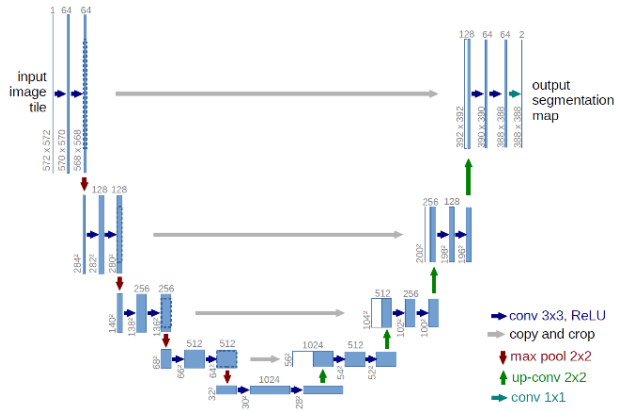

FIGURE 7. U-net.

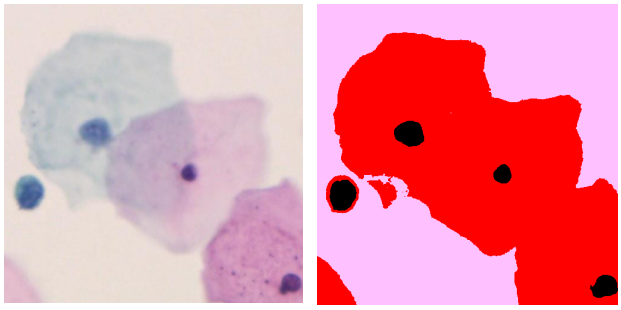

FIGURE 8. Result of semantic segmentation.

U-Net, the other semantic segmentation networks, is famous for its encoder and decoder architecture with skip connections to mitigate the issue of vanishing gradients, enabling effective capture of spatial information while maintaining high-resolution output. The architecture and segmentation results are depicted in Figure 7 and Figure 8, respectively. While this architecture efficiently captures rough contours of cell nuclei and cytoplasm, cannot classify overlapping pixels [134]. As a result, they often require post-processing to extract individual complete cells from overlapping regions. Zhang et al. [88] utilized U-Net with soft Attention Gates (AG) to capture detailed information from deep layers for accurate nuclei prediction. They then constructed polar coordinates based on the nuclei to detect cell boundaries, followed by refining them using a graph-based Random Walk. Mahyari and Dansereau [55] combines the cytoplasmic region using the results of two methods: the first is based on CNN, and the second is generated using a multi-layer random walker based on nuclei. These two results are integrated using the Hungarian algorithm. Riana et al. [135] utilized a UNet model with VGG encoders to detect areas of cytoplasm and regions of overlapping cells, refining the results using the Watershed method. Zhang et al. [136] utilized ResNet-101 for cell

TABLE 6. Summary of semantic segmentation methods.

Reference	Datasets	Methods	Evaluation
Segmentation of nuclei in overlapping cells			
[141]	ISBI 2014	CNN	Rec: 91.7% Prec: 92.9%
[40]	ISBI 2014 ISBI 2015	ResNeXt Binary tree-like network, Two-path fusion attention	Prec: 0.90 Rec: 0.94 F1: 0.93
[137]	ISBI 2014	U-net Context encoding layer, Attention learning module, Prior knowledge	AJI: 0.7908 PQ: 0.7718 DC: 0.8981 HD: 26.6950
[142]	265 slides 2048x2048	U-Net Multiscale Context Gating Residual Block, Global Context Attention Block, Multikernel Maxpooling Residual Block	AJI: 0.684 DC: 0.88 PQ: 0.688
[53]	ISBI 2014 ISBI 2015	U-Net Cross-scale features integration, Two interconnected decoders	Object-level: Acc: 93% Rec: 95.32% Pixel-level: Acc: 92.56%, Rec: 92.27% DC: 93.12% F1: 94.96%
[140]	ISBI 2014	Squeeze and Excitation (SE) block, U-Net	Prec: 98.32 Rec: 97.18
Segmentation of overlapping Nuclei			
[43]	CNSeg	AL-net Grabcut	AJI PatchSeg: 0.7186 ClusterSeg: 0.6958 PQ PatchSeg: 0.7064 ClusterSeg: 0.6909
Delineation of ROI			
[66]	2000x2000 training: 767 testing: 315	FCN-8 and FCN-16	Sens: 0.6613 Spec: 0.9615 Acc: 0.8667 IoU: 0.5344
[143]	194 images	CNN	Prec: 0.73 Rec: 0.65
Segmentation of overlapping cells			
[144]	ISBI 2015	Multi-scale CNN Multiple Cells Labeling, Dynamic multi-template Deformation model	DC: 0.89
[70]	ISBI 2014	SLIC CNN Voronoi Level Set Shape prior Model	Nuclei Prec: 0.994 Rec: 0.911 Cyto: ZSI: 0.90
[117]	ISBI 2014 ISBI 2015	TernausNet DeepLab V2 Conditional random fields DRLSE	DC: 0.92
[118]	ISBI 2014	U-Net DRLSE Distance map and shape prior	DC Nuclei: 0.94 Cyto: 0.89
[145]	ISBI 2015	Multi-scale CNN Adaptive shape priors	DC overlapping degree (0,0.3]: 0.84
[54]	ISBI 2015 280 images based on EDF	K-means U-net	DC: 0.872
[88]	ISBI 2014	ATT U-Net Polar coordinate Graph-based Random Walk	DC Nuclei: 0.93 Cyto: 0.93

TABLE 6. *(Conitnued.)* **Summary of semantic segmentation methods.**

[56]	ISBI 2014 50000 synthetic	Two-stage CNN Skip connections. Residual blocks Beer-Lambert law	Acc: 99.87 IOU: 96.95
[55]	ISBI 2014 and 100,000 new images from ISBI 2014	CNN Random walker Region growing	DC: 0.968
[135]	RepomedUNM	VGG-UNet Watershed	IoU: 90.61
[136]	CCEDD	ResNet-101 Mask Guidance Module, Refinement Aggregated Module	AP: 0.763
[134]	Cx22	U-Net and U-Net++, Encoders: Resnet34 and DenseNet121	Cyto: DC: 0.9535 Sens: 0.9621 Spec: 0.9835 Nuclei: DC: 0.7863 Sens: 0.9581 Spec: 0.9961
[146]	311 cells	U-Net Radius tracking	Prec:0.8895 Rec:0.7783 DC: 0.8302 IoU:0.7413

boundary detection, utilizing a global feature pyramid to acquire the global context and multi-scale features of both semantics and edges. They then leveraged the complementarity between semantics and edges to enhance the accuracy of segmentation.

Furthermore, recent advancements in feature extraction methods and modules have significantly enhanced segmentation performance. Jianwei Zhang et al. [40] introduced a Binary Tree-like Network that integrates nucleus features extracted from 5-layer of ResNeXt. These features are subsequently fused using attention to generate the final feature map. Zhao et al. [137] introduced an encoder-decoder network with integrated attention-learning modules within skip connections, complemented by a context encoding layer within the encoder. This architecture facilitates the extraction of contextual information across various resolutions, incorporating both contextual and attention mechanisms for nucleus segmentation. Yang et al. [138] utilized the Gating Context-aware Pooling module to enhance the model's ability to perceive long-range dependencies and global context. They used a pre-trained ResNet-34 model as an encoder and a decoder with a Global Context Attention (GCA) block for nucleus detection. Luo et al. [139] presented a dual-supervised network for nuclei segmentation from whole-slide images (WSI). The autoencoder comprises a down-sampling network and a super-resolution network. A feature extraction module, employing a residual network, extracts semantic information. The decoding module integrates feature fusion, segmentation, and edge detection techniques for precise nuclei segmentation within WSI. This approach achieves equivalent segmentation accuracy while offering a five-fold increase in speed compared to U-Net. Chowdary and Yogarajah [140] proposed an encoder-decoder architecture for nuclei segmentation in images. They enhanced the network by replacing convolutional layers with a combination of residual blocks and Squeeze-and-Excitation (SE) module. This modification aimed to enhance the ability to discern between local and global information. Rasheed et al. [53] introduced a C-UNet for the segmentation of cervical nuclei. This architecture integrates features from diverse spatial resolutions and domains using a Cross-scale features integration (CSFI) module. Boundary detection and semantic segmentation is based on two interconnected linked decoders. Ji et al. [134] employed multiple semantic segmentation methods, including U-Net and U-Net++, for nucleus and cytoplasm segmentation using the Cx22 dataset. They generated final predictions by applying an unweighted average ensemble method to combine results from multiple models. This approach does not involve post-processing to segment overlapping regions. Table 6 summarizes the methods employed in semantic segmentation along with their performance evaluation.

2) INSTANCE SEGMENTATION

Instance segmentation uses masks to detect targets, enabling multiple detections of individual pixels, which aligns with the logic of overlapping regions where a single pixel may belong to multiple cell instances. In contrast, semantic

segmentation assigns each pixel to only one semantic category.

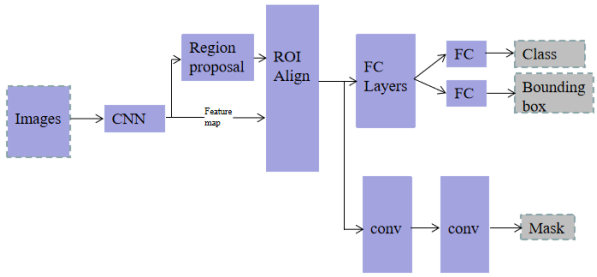

FIGURE 9. Mask R-CNN.

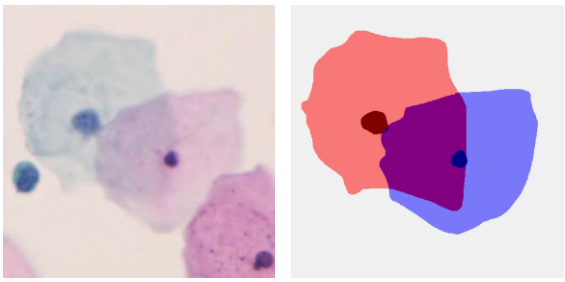

FIGURE 10. Original image and instance segmentation result.

Mask R-CNN expands the Faster R-CNN network by introducing an extra branch to predict segmentation masks [147]. The architecture and the instance segmentation result are depicted in Figure 9 and Figure 10, respectively. This allows Mask R-CNN to generate pixel-level masks for each detected object, enabling accurate delineation of object boundaries and precise segmentation. Additionally, the two-stage architecture of Mask R-CNN, with separate region proposal and refinement stages, enhances both speed and accuracy,

Chen and Zhang [148] utilized Mask R-CNN for segmenting overlapping cells. Zhou et al. [149] employed Mask R-CNN along with the Duplicate Removal Module and Instance Relation Module to achieve improved performance. Following that, they presented a deep semi-supervised framework for overlapped cell segmentation. This framework includes a teacher branch and a student branch, both built upon the backbone architecture of Mask R-CNN [150]. Jiang et al. [151] segmented overlapping cells into Intersection Layer and Complement Layer using Mask R-CNN, and then recombined overlapping and non-overlapping regions using the Semantic Consistency guided Recombination Module. Liu et al. [42] created a dataset of cervical cytology images called Cx22, comprising the boundaries of 14,946 cell instances from 1320 images. They introduced a region-of-interest (ROI) based label cropping algorithm for annotation using the annotation tool, LabelMe. Additionally, they proposed both semantic and instance segmentation methods as baseline approaches. Zhao et al. [133] proposed using Residual Attention Embedding (RAE) blocks to focus on cell boundaries, employing two heads: one for object probability and another for polygon distance prediction. They completed instance segmentation using post-processing techniques. Summary of instance segmentation methods is provided in Table 7.

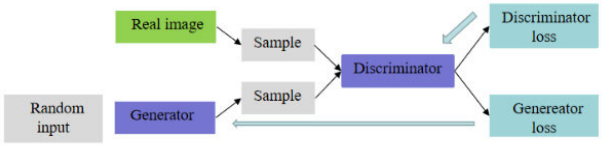

FIGURE 11. GAN.

3) GANs

Generative Adversarial Networks (GANs) [155], proposed by Goodfellow in 2014, operates as a two-player game involving a generator and discriminator. The generator learns to produce synthetic instances that closely mimic authentic data, whereas the discriminator is trained to distinguish genuine examples from artificial ones. Hao et al. [156] introduced a two-stage segmentation approach: first, a cellular region proposal network for coarse segmentation of nuclei and cytoplasm, followed by a pixel-level segmentation network utilizing a GAN-based model to enhance segmentation accuracy. Huang et al. [142] introduced Cell-GAN, which segments cells based on guiding factors such as the nucleus. In Cell-GAN, non-overlapping cellular components are considered as the background. The generator is responsible for producing segmented cell images, while the discriminator learns the probability distribution of cells by assessing the variance between segmented images and ground truth. Moreover, Cell-GAN utilizes the nucleus as a guiding factor for cell localization. Both methods involve cropping the input image into small sizes. The architecture of GAN is shown in Figure 11, with the evaluations of GANs-based approaches summarized in Table 8.

IV. DISSCUSSION AND CHALLENGES

A. DATASETS

High-quality datasets are crucial for cell segmentation. Although the ISBI dataset, one of the earliest released open-source datasets, has a small amount of data, it has been widely used due to its accuracy and has become an established benchmark dataset. Following a comprehensive investigation, the existing datasets utilized for overlapping cervical cell segmentation demonstrate several key characteristics. First, data imbalance is a common issue, as cells typically occupy only a small portion of the image, leading to sample imbalance during training. Additionally, the diversity of data styles due to varying staining techniques and imaging methods results in significant differences in color, size, and image resolution. These factors lead to different magnification levels and a mixture of color and grayscale images. Moreover, the labels are diverse; cell nuclei, having prominent visual features, are relatively easy to label, whereas cell cytoplasm is more challenging to delineate accurately due to overlapping

TABLE 7. Summary of instance segmentation methods.

Reference	Datasets	Methods	Evaluation
Segment nuclei in overlapping cells			
[152]	Personal 178 images 3048×2048	Mask R-CNN	Nuclei: Acc: 89.8% Sens: 72.5% Spec: 94.3%
Segmentation of overlapping cells			
[148]	ISBI 2014 ISBI 2015	Mask RCNN	DC: 0.92
[149]	CPS	Mask RCNN Duplicate Removal Module, Instance Relation Module	F1 Cyto: 0.7497 Nuclei:0.7554
[153]	680 LBC 1280*1024 pixels	multi-semantic label model Faster R-CNN	×
[150]	Personal 4439 cytoplasm and 4789 nuclei	Mask R-CNN Mean Teacher algorithm Mask-Guided Feature Distillation	mAP Cyto.: 46.01 Nuc.: 35.02 Avg.: 40.52
[154]	6451 cells	PolarMask extends two polar branches Non-Maximum Suppression	Cell: success rate = 0.9 when DC > 0.5
[42]	Cx22	UNet, UNet++, Unet3+ and Mask R-CNN	DC Cyto: 0.948 Nuclei: 0.750
[133]	ISBI 14 3260 images 256×256	Encoder-decoder Residual-based attentional embedding (RAE) block, PA-NMS	DC: 92.57% TPp: 86.78% FPp: 0.19% FN: 5.46% AP: 89.45%
[151]	ISBI2014 CPS	Mask R-CNN, Semantic Consistency Recombination Module	ISBI2014 mAP: 64.02 DC: 92.13 CPS mAP: 49.65 DC: 89.50

TABLE 8. Summary of GANs methods.

Reference	Datasets	Methods	Evaluation
[57]	Personal 44889 images	cGAN generator: U-Net combining DenseBlock	Correlation coefficient: 0.9910
[156]	ISBI 2014	OHEM + Soft-NMS GAN	Nucleus Prec: 0.902 Rec: 0.982 ZSI: 0.940 Cytoplasm DC: 0.920
[142]	ISBI 2015	GAN Recurrent Image Cropping	DC: 0.899

cells, low contrast, and staining issues, adding complexity to the segmentation task. Finally, the data volumes vary widely, with sample sizes ranging from hundreds to tens of thousands.

Based on this analysis, several challenges related to datasets need to be addressed. Privacy issues limit data acquisition, resulting in a scarcity of available data. Additionally, the diversity of data, including variations in staining techniques, data acquisition methods, and imaging specifications, lacks unified standards, complicating data integration and comparison. The same issues also arise in the acquisition of EDF images and the definition of overlap degree. Furthermore, the processes of data collection and annotation require specialized personnel and tools, making them both time-consuming and labor-intensive, which results in a shortage of large-scale data.

B. METHODS

We categorize the machine learning methods for overlapping cell segmentation into two types: conventional machine learning and deep learning.

Conventional machine learning methods rely on handcrafted features designed and extracted based on prior knowledge for induction and feature selection. Due to the absence of a one-size-fits-all tool, a combination of multiple methods and stages is typically necessary, including preprocessing, coarse segmentation, and fine segmentation. Region-based methods and pixel intensity-based methods are commonly employed for coarse segmentation to identify the approximate areas of cells. For accurate segmentation of overlapping regions, contour-based methods, such as level set and its variants, are used. These methods require high-quality data, and their performance and accuracy are often limited. Data enhancement techniques, primarily focusing on smoothing, denoising, and contrast enhancement, aim to improve model capabilities. While these methods offer good interpretability, they often struggle with complex datasets.

Deep learning methods, characterized by their multilayered architectures and millions of parameters, possess the capacity to fit almost any dataset. As the dataset size increases, models can learn richer features and patterns from a wider variety of samples, thereby reducing the likelihood of overfitting. Data augmentation plays a significant role in deep learning, with common techniques including rotation, flipping, and other transformations. Additionally, pre-trained models are extensively utilized in deep learning applications. These methods, such as data augmentation and pre-training, are generally not applicable to conventional machine learning approaches.

Deep learning methods are increasingly becoming the mainstream approach in the field of overlapping cell segmentation, but there is still potential for improvement in segmentation performance. Advanced feature extraction networks, particularly those that incorporate attention mechanisms, significantly enhance the model's capability to capture relevant features in complex datasets. On the other hand, considerations regarding model complexity and efficiency are crucial; the scale of network parameters and the speed of training and inference directly impact the practical applicability of deep learning models.

C. PRACTICAL IMPLEMENTATION

In medical imaging, segmentation involves not only isolating cell or lesion areas from images but also providing precise diagnostic insights for clinicians. This highlights the importance of segmentation outcomes seamlessly integrating with other processes, such as data acquisition enhancement and final classification, to ensure accurate diagnostic conclusions. Hence, segmentation tasks must not only prioritize technical accuracy and efficiency but also align with the broader medical image analysis workflow to enhance diagnostic efficacy.

V. CONCLUSION

In this comprehensive survey, we present a detailed overview of overlapping cervical cell segmentation, encompassing datasets, evaluation methods, and techniques for nuclei and cytoplasm segmentation. we utilized the specified algorithm to segment overlapping cells, demonstrating its effectiveness and making the algorithm easier to understand through detailed visual results. In the task of cell boundary detection, methods are classified into two classes: conventional machine learning and deep learning approaches. The most used methods in conventional machine learning are superpixel, thresholding, and level set method. Semantic methods require post-processing to address overlapping regions, while instance segmentation offers a direct approach to segment overlapping cells. Although GANs have been utilized in this domain, their applicability is constrained by specific conditions. This summary underscores the diverse methodologies employed in overlapping cell segmentation, illustrating ongoing efforts to enhance accuracy and efficiency in biomedical image analysis.

ACKNOWLEDGMENT

E Chen would like to thank Dr. Jun Bai for his invaluable inspiration and assistance with this article. E Chen also deeply appreciate the reviewers for their in-depth and comprehensive comments.

REFERENCES

[1] H. Sung, J. Ferlay, R. L. Siegel, M. Laversanne, I. Soerjomataram, A. Jemal, and F. Bray, "Global cancer statistics 2020: GLOBOCAN estimates of incidence and mortality worldwide for 36 cancers in 185 countries," *CA, A Cancer J. Clinicians*, vol. 71, no. 3, pp. 209–249, Feb. 2021.

[2] P. A. Cohen, A. Jhingran, A. Oaknin, and L. Denny, "Cervical cancer," *Lancet*, vol. 393, no. 10167, pp. 169–182, Jan. 2019.

[3] N. F. Schlecht, "Human papillomavirus infection and time to progression and regression of cervical intraepithelial neoplasia," *CancerSpectrum Knowl. Environ.*, vol. 95, no. 17, pp. 1336–1343, Sep. 2003.

[4] V. Bouvard, N. Wentzensen, A. Mackie, J. Berkhof, J. Brotherton, P. Giorgi-Rossi, R. Kupets, R. Smith, S. Arrossi, K. Bendahhou, and K. Canfell, "The IARC perspective on cervical cancer screening," *New England J. Med.*, vol. 385, no. 20, pp. 1908–1918, Nov. 2021.

[5] F. L. Kitchen and C. M. Cox, *Papanicolaou Smear*. Treasure Island, FL, USA: StatPearls, 2022.

[6] M. Kang, S. Y. Ha, H. Y. Cho, D. H. Chung, N. R. Kim, J. An, S. Lee, J. Y. Seok, and J. Jeong, "Comparison of papanicolaou smear and human papillomavirus (HPV) test as cervical screening tools: Can we rely on HPV test alone as a screening method? An 11-year retrospective experience at a single institution," *J. Pathol. Translational Med.*, vol. 54, no. 1, pp. 112–118, Jan. 2020.

[7] P. Sathawane, M. M. Kamal, P. R. Deotale, and H. Mankar, "Nuances of the papanicolaou stain," *Cytojournal*, vol. 19, p. 43, Jun. 2022.

[8] M. Kamal, "Pap smear collection and preparation: Key points," *Cytojournal*, vol. 19, p. 24, Mar. 2022.

[9] P. N. Staats, R. J. Souers, A. L. Nunez, Z. Li, D. F. I. Kurtycz, K. Goodrich, B. L. Witt, D. D. Davey, and C. N. Booth, "The differential diagnosis of reparative changes and malignancy: Performance in the college of American pathologists pap education and proficiency testing programs," *Arch. Pathol. Lab. Med.*, vol. 144, no. 7, pp. 846–852, Jul. 2020.

[10] M. A. Pangarkar, "The Bethesda system for reporting cervical cytology," *Cytojournal*, vol. 19, p. 28, Apr. 2022.

[11] Y. Xiang, W. Sun, C. Pan, M. Yan, Z. Yin, and Y. Liang, "A novel automation-assisted cervical cancer reading method based on convolutional neural network," *Biocybernetics Biomed. Eng.*, vol. 40, no. 2, pp. 611–623, Apr. 2020.

[12] O. Attallah, "CerCan·Net: Cervical cancer classification model via multi-layer feature ensembles of lightweight CNNs and transfer learning," *Exp. Syst. Appl.*, vol. 229, Nov. 2023, Art. no. 120624.
[13] Z. Alyafeai and L. Ghouti, "A fully-automated deep learning pipeline for cervical cancer classification," *Exp. Syst. Appl.*, vol. 141, Mar. 2020, Art. no. 112951.
[14] A. Ghoneim, G. Muhammad, and M. S. Hossain, "Cervical cancer classification using convolutional neural networks and extreme learning machines," *Future Gener. Comput. Syst.*, vol. 102, pp. 643–649, Jan. 2020.
[15] K. Adem, S. Kiliçarslan, and O. Cömert, "Classification and diagnosis of cervical cancer with stacked autoencoder and softmax classification," *Exp. Syst. Appl.*, vol. 115, pp. 557–564, Jan. 2019.
[16] N. Dong, L. Zhao, C. H. Wu, and J. F. Chang, "Inception V3 based cervical cell classification combined with artificially extracted features," *Appl. Soft Comput.*, vol. 93, Aug. 2020, Art. no. 106311.
[17] M. M. Ali, K. Ahmed, F. M. Bui, B. K. Paul, S. M. Ibrahim, J. M. W. Quinn, and M. A. Moni, "Machine learning-based statistical analysis for early stage detection of cervical cancer," *Comput. Biol. Med.*, vol. 139, Dec. 2021, Art. no. 104985.
[18] M. M. Rahaman, C. Li, Y. Yao, F. Kulwa, X. Wu, X. Li, and Q. Wang, "DeepCervix: A deep learning-based framework for the classification of cervical cells using hybrid deep feature fusion techniques," *Comput. Biol. Med.*, vol. 136, Sep. 2021, Art. no. 104649.
[19] S. Fekri-Ershad and S. Ramakrishnan, "Cervical cancer diagnosis based on modified uniform local ternary patterns and feed forward multilayer network optimized by genetic algorithm," *Comput. Biol. Med.*, vol. 144, May 2022, Art. no. 105392.
[20] N. Patel, R. Bavikar, A. Buch, M. Kulkarni, A. Dharwadkar, and V. Viswanathan, "A comparison of conventional pap smear and liquid-based cytology for cervical cancer screening," *Gynecol. Minimally Invasive Therapy*, vol. 12, no. 2, pp. 77–82, 2023.
[21] R. Gupta, R. Yadav, A. Sharda, D. Kumar, R. Mehrotra, and S. Gupta, "Comparative evaluation of conventional cytology and a low-cost liquid-based cytology technique, EziPREP, for cervicovaginal smear reporting: A split sample study," *CytoJournal*, vol. 16, p. 22, Nov. 2019.
[22] T. P. Deepa and A. N. Rao, "Classification of normal and abnormal overlapped squamous cells in pap smear image," *Int. J. Syst. Assurance Eng. Manage.*, vol. 15, no. 1, pp. 519–531, Jan. 2023.
[23] M. Guven and C. Cengizler, "Data cluster analysis-based classification of overlapping nuclei in pap smear samples," *Biomed. Eng. OnLine*, vol. 13, no. 1, p. 159, 2014.
[24] E. Bengtsson, O. Eriksson, J. Holmquist, T. Jarkrans, B. Nordin, and B. Stenkvist, "Segmentation of cervical cells: Detection of overlapping cell nuclei," *Comput. Graph. Image Process.*, vol. 16, no. 4, pp. 382–394, Aug. 1981.
[25] Z. Hu, J. Tang, Z. Wang, K. Zhang, L. Zhang, and Q. Sun, "Deep learning for image-based cancer detection and diagnosis? A survey," *Pattern Recognit.*, vol. 83, pp. 134–149, Nov. 2018.
[26] N. Kumaresan and D. Somasundaram, "Review of pap smears cell segmentation and classification techniques for cervical cancer analysis," *Stud. Ethno-Medicine*, vol. 12, no. 2, pp. 96–105, Nov. 2018.
[27] W. William, A. Ware, A. H. Basaza-Ejiri, and J. Obungoloch, "A review of image analysis and machine learning techniques for automated cervical cancer screening from pap-smear images," *Comput. Methods Programs Biomed.*, vol. 164, pp. 15–22, Oct. 2018.
[28] C. Li, H. Chen, X. Li, N. Xu, Z. Hu, D. Xue, S. Qi, H. Ma, L. Zhang, and H. Sun, "A review for cervical histopathology image analysis using machine vision approaches," *Artif. Intell. Rev.*, vol. 53, no. 7, pp. 4821–4862, Oct. 2020.
[29] M. M. Rahaman, C. Li, X. Wu, Y. Yao, Z. Hu, T. Jiang, X. Li, and S. Qi, "A survey for cervical cytopathology image analysis using deep learning," *IEEE Access*, vol. 8, pp. 61687–61710, 2020.
[30] A. Sarwar, A. A. Sheikh, J. Manhas, and V. Sharma, "Segmentation of cervical cells for automated screening of cervical cancer: A review," *Artif. Intell. Rev.*, vol. 53, no. 4, pp. 2341–2379, Apr. 2020.
[31] A. Halim, W. Azani Mustafa, W. Khairunizam Wan Ahmad, H. A. Rahim, and H. Sakeran, "Nucleus detection on pap smear images for cervical cancer diagnosis: A review analysis," *Oncologie*, vol. 23, no. 1, pp. 73–88, 2021.
[32] H. Jiang, Y. Zhou, Y. Lin, R. C. K. Chan, J. Liu, and H. Chen, "Deep learning for computational cytology: A survey," *Med. Image Anal.*, vol. 84, Feb. 2023, Art. no. 102691.
[33] G. Litjens, T. Kooi, B. E. Bejnordi, A. A. A. Setio, F. Ciompi, M. Ghafoorian, J. A. Van Der Laak, B. Van Ginneken, and C. I. Sánchez, "A survey on deep learning in medical image analysis," *Med. Image Anal.*, vol. 42, pp. 60–88, Dec. 2017.
[34] T. Conceição, C. Braga, L. Rosado, and M. J. M. Vasconcelos, "A review of computational methods for cervical cells segmentation and abnormality classification," *Int. J. Mol. Sci.*, vol. 20, no. 20, p. 5114, Oct. 2019.
[35] M. E. Plissiti and C. Nikou, "A review of automated techniques for cervical cell image analysis and classification," in *Biomedical Imaging and Computational Modeling in Biomechanics*. Berlin, Germany: Springer, 2013, pp. 1–18.
[36] A. V. Matias, J. G. A. Amorim, L. A. B. Macarini, A. Cerentini, A. S. C. Onofre, F. B. D. M. Onofre, F. P. Daltoé, M. R. Stemmer, and A. von Wangenheim, "What is the state of the art of computer vision-assisted cytology? A systematic literature review," *Computerized Med. Imag. Graph.*, vol. 91, Jul. 2021, Art. no. 101934.
[37] Z. Lu, G. Carneiro, and A. P. Bradley, "An improved joint optimization of multiple level set functions for the segmentation of overlapping cervical cells," *IEEE Trans. Image Process.*, vol. 24, no. 4, pp. 1261–1272, Apr. 2015.
[38] Z. Lu, G. Carneiro, A. P. Bradley, D. Ushizima, M. S. Nosrati, A. G. C. Bianchi, C. M. Carneiro, and G. Hamarneh, "Evaluation of three algorithms for the segmentation of overlapping cervical cells," *IEEE J. Biomed. Health Informat.*, vol. 21, no. 2, pp. 441–450, Mar. 2017.
[39] H. Ahmady Phoulady and P. R. Mouton, "A new cervical cytology dataset for nucleus detection and image classification (Cervix93) and methods for cervical nucleus detection," 2018, *arXiv:1811.09651*.
[40] J. Zhang, Z. Liu, B. Du, J. He, G. Li, and D. Chen, "Binary tree-like network with two-path fusion attention feature for cervical cell nucleus segmentation," *Comput. Biol. Med.*, vol. 108, pp. 223–233, May 2019.
[41] J. Liu, H. Fan, Q. Wang, W. Li, Y. Tang, D. Wang, M. Zhou, and L. Chen, "Local label point correction for edge detection of overlapping cervical cells," 2020, *arXiv:2010.01919*.
[42] G. Liu, Q. Ding, H. Luo, M. Sha, X. Li, and M. Ju, "cx22: A new publicly available dataset for deep learning-based segmentation of cervical cytology images," *Comput. Biol. Med.*, vol. 150, Nov. 2022, Art. no. 106194.
[43] J. Zhao, Y.-J. He, S.-H. Zhou, J. Qin, and Y.-N. Xie, "CNSeg: A dataset for cervical nuclear segmentation," *Comput. Methods Programs Biomed.*, vol. 241, Nov. 2023, Art. no. 107732.
[44] N. Awasthi, P. Katare, S. S. Gorthi, and P. K. Yalavarthy, "Guided filter based image enhancement for focal error compensation in low cost automated histopathology microscopic system," *J. Biophotonics*, vol. 13, no. 11, Nov. 2020, Art. no. e202000123.
[45] P. Malm, B. N. Balakrishnan, V. K. Sujathan, R. Kumar, and E. Bengtsson, "Debris removal in pap-smear images," *Comput. Methods Programs Biomed.*, vol. 111, no. 1, pp. 128–138, Jul. 2013.
[46] S. Haridas and T. Jayamalar, "PAP smear image enhancement using diffusion stop function based clahe algorithm," in *Proc. 8th Int. Conf. Adv. Comput. Commun. Syst. (ICACCS)*, vol. 1, Coimbatore, India, Mar. 2022, pp. 1048–1054.
[47] Y. Song, J.-Z. Cheng, D. Ni, S. Chen, B. Lei, and T. Wang, "Segmenting overlapping cervical cell in pap smear images," in *Proc. IEEE 13th Int. Symp. Biomed. Imag. (ISBI)*, Prague, Czech Republic, Apr. 2016, pp. 1159–1162.
[48] T. Guan, D. Zhou, and Y. Liu, "Accurate segmentation of partially overlapping cervical cells based on dynamic sparse contour searching and GVF snake model," *IEEE J. Biomed. Health Informat.*, vol. 19, no. 4, pp. 1494–1504, Jul. 2015.
[49] S. Kaur and J. S. Sahambi, "Curvelet initialized level set cell segmentation for touching cells in low contrast images," *Computerized Med. Imag. Graph.*, vol. 49, pp. 46–57, Apr. 2016.
[50] A. Gençtav, S. Aksoy, and S. Önder, "Unsupervised segmentation and classification of cervical cell images," *Pattern Recognit.*, vol. 45, no. 12, pp. 4151–4168, Dec. 2012.
[51] L. Zhang, H. Kong, C. T. Chin, S. Liu, Z. Chen, T. Wang, and S. Chen, "Segmentation of cytoplasm and nuclei of abnormal cells in cervical cytology using global and local graph cuts," *Computerized Med. Imag. Graph.*, vol. 38, no. 5, pp. 369–380, Jul. 2014.
[52] L. Zhang, S. Chen, T. Wang, Y. Chen, S. Liu, and M. Li, "A practical segmentation method for automated screening of cervical cytology," in *Proc. Int. Conf. Intell. Comput. Bio-Medical Instrum.*, Hubei, China, Dec. 2011, pp. 140–143.

[53] A. Rasheed, S. H. Shirazi, A. I. Umar, M. Shahzad, W. Yousaf, and Z. Khan, "Cervical cell's nucleus segmentation through an improved UNet architecture," *PLoS ONE*, vol. 18, no. 10, Oct. 2023, Art. no. e0283568.

[54] A. Umadi, K. Nagarajan, J. B. Venkatesha, A. Ganesh, and K. George, "Automated segmentation of overlapping cells in cervical cytology images using deep learning," in *Proc. IEEE 17th India Council Int. Conf. (INDICON)*, New Delhi, India, Dec. 2020, pp. 1–7.

[55] T. L. Mahyari and R. M. Dansereau, "Multi-layer random Walker image segmentation for overlapped cervical cells using probabilistic deep learning methods," *IET Image Process.*, vol. 16, no. 11, pp. 2959–2972, Sep. 2022.

[56] T. L. Mahyari and R. M. Dansereau, "Deep learning methods for image decomposition of cervical cells," in *Proc. 28th Eur. Signal Process. Conf. (EUSIPCO)*, Amsterdam, The Netherlands, Jan. 2021, pp. 1110–1114.

[57] X. Geng, S. Liua, W. Han, X. Li, J. Ma, J. Yu, X. Liu, S. Zeng, L. Chen, and S. Cheng, "FFusionCGAN: An end-to-end fusion method for few-focus images using conditional GAN in cytopathological digital slides," 2020, *arXiv:2001.00692*.

[58] R. Achanta, A. Shaji, K. Smith, A. Lucchi, P. Fua, and S. Süsstrunk, "SLIC superpixels compared to state-of-the-art superpixel methods," *IEEE Trans. Pattern Anal. Mach. Intell.*, vol. 34, no. 11, pp. 2274–2282, Nov. 2012.

[59] A. Tareef, Y. Song, W. Cai, D. D. Feng, and M. Chen, "Automated three-stage nucleus and cytoplasm segmentation of overlapping cells," in *Proc. 13th Int. Conf. Control Autom. Robot. Vis. (ICARCV)*, Dec. 2014, pp. 865–870.

[60] H. Lee and J. Kim, "Segmentation of overlapping cervical cells in microscopic images with superpixel partitioning and cell-wise contour refinement," in *Proc. IEEE Conf. Comput. Vis. Pattern Recognit. Workshops (CVPRW)*, Las Vegas, NV, USA, Jun. 2016, pp. 1367–1373.

[61] D. N. Diniz, R. F. Vitor, A. G. C. Bianchi, S. Delabrida, C. M. Carneiro, D. M. Ushizima, F. N. S. de Medeiros, and M. J. F. Souza, "An ensemble method for nuclei detection of overlapping cervical cells," *Exp. Syst. Appl.*, vol. 185, Dec. 2021, Art. no. 115642.

[62] Y. Song, L. Zhang, S. Chen, D. Ni, B. Li, Y. Zhou, B. Lei, and T. Wang, "A deep learning based framework for accurate segmentation of cervical cytoplasm and nuclei," in *Proc. 36th Annu. Int. Conf. IEEE Eng. Med. Biol. Soc.*, Chicago, IL, USA, Aug. 2014, pp. 2903–2906.

[63] S. Tello-Mijares, J. Bescós, and F. Flores, "Nuclei segmentation and identification in practical pap-smear images with multiple overlapping cells," *J. Med. Imag. Health Informat.*, vol. 6, no. 4, pp. 992–1000, Aug. 2016.

[64] P. Wang, L. Wang, Y. Li, Q. Song, S. Lv, and X. Hu, "Automatic cell nuclei segmentation and classification of cervical pap smear images," *Biomed. Signal Process. Control*, vol. 48, pp. 93–103, Feb. 2019.

[65] R. Saha, M. Bajger, and G. Lee, "Segmentation of cervical nuclei using SLIC and pairwise regional contrast," in *Proc. 40th Annu. Int. Conf. IEEE Eng. Med. Biol. Soc. (EMBC)*, Honolulu, HI, USA, Jul. 2018, pp. 3422–3425.

[66] B. Harangi, J. Toth, G. Bogacsovics, D. Kupas, L. Kovacs, and A. Hajdu, "Cell detection on digitized pap smear images using ensemble of conventional image processing and deep learning techniques," in *Proc. 11th Int. Symp. Image Signal Process. Anal. (ISPA)*, Dubrovnik, Croatia, Sep. 2019, pp. 38–42.

[67] D. M. Ushizima, A. G. Bianchi, and C. M. Carneiro, "Segmentation of subcellular compartments combining superpixel representation with Voronoi diagrams," in *Proc. Int. Symp. Biomed. Imag.*, 2015, pp. 1–2.

[68] A. Khadidos, V. Sanchez, and C.-T. Li, "Patch-based segmentation of overlapping cervical cells using active contour with local edge information," in *Proc. IEEE Int. Conf. Acoust., Speech Signal Process. (ICASSP)*, New Orleans, LA, USA, Mar. 2017, pp. 1058–1062.

[69] Z. Lu, G. Carneiro, and A. P. Bradley, "Automated nucleus and cytoplasm segmentation of overlapping cervical cells," in *Proc. MICCAI* Nagoya, Japan, Sep. 2013, pp. 452–460.

[70] A. Tareef, Y. Song, W. Cai, H. Huang, H. Chang, Y. Wang, M. Fulham, D. Feng, and M. Chen, "Automatic segmentation of overlapping cervical smear cells based on local distinctive features and guided shape deformation," *Neurocomputing*, vol. 221, pp. 94–107, Jan. 2017.

[71] Y. Li, Q. Wang, X. Fan, X. Xu, and J. Gong, "A framework for cervical cell EDF image segmentation using similarity measure," in *Proc. 39th Chin. Control Conf. (CCC)*, Shenyang, China, Jul. 2020, pp. 6503–6508.

[72] G. Liu, Q. Ding, H. Luo, M. Ju, T. Jin, M. He, and G. Dong, "A novel evolution strategy of level set method for the segmentation of overlapping cervical cells," *Appl. Sci.*, vol. 11, no. 1, p. 443, Jan. 2021.

[73] G. L. Ramalho, D. S. Ferreira, A. G. Bianchi, C. M. Carneiro, F. N. Medeiros, and D. M. Ushizima, "Cell reconstruction under Voronoi and enclosing ellipses from 3D microscopy," in *Proc. ISBI*, Brooklyn, NY, USA, Apr. 2015, pp. 1–2.

[74] J. Zhang, Z. Hu, G. Han, and X. He, "Segmentation of overlapping cells in cervical smears based on spatial relationship and overlapping translucency light transmission model," *Pattern Recognit.*, vol. 60, pp. 286–295, Dec. 2016.

[75] A. Tareef, Y. Song, H. Huang, D. Feng, M. Chen, Y. Wang, and W. Cai, "Multi-pass fast watershed for accurate segmentation of overlapping cervical cells," *IEEE Trans. Med. Imag.*, vol. 37, no. 9, pp. 2044–2059, Sep. 2018.

[76] Y. Song, L. Zhang, S. Chen, D. Ni, B. Lei, and T. Wang, "Accurate segmentation of cervical cytoplasm and nuclei based on multiscale convolutional network and graph partitioning," *IEEE Trans. Biomed. Eng.*, vol. 62, no. 10, pp. 2421–2433, Oct. 2015.

[77] A. Tareef, Y. Song, H. Huang, Y. Wang, D. Feng, M. Chen, and W. Cai, "Optimizing the cervix cytological examination based on deep learning and dynamic shape modeling," *Neurocomputing*, vol. 248, pp. 28–40, Jul. 2017.

[78] H.-G. Lee and S.-C. Lee, "Nucleus segmentation using Gaussian mixture based shape models," *IEEE J. Biomed. Health Informat.*, vol. 22, no. 1, pp. 235–243, Jan. 2018.

[79] S. N. Sulaiman, N. A. M. Isa, I. A. Yusoff, and N. H. Othman, "Overlapping cells separation method for cervical cell images," in *Proc. 10th Int. Conf. Intell. Syst. Design Appl.*, Cairo, Egypt, Nov. 2010, pp. 1218–1222.

[80] H. A. Phoulady, D. Goldgof, L. O. Hall, and P. R. Mouton, "A framework for nucleus and overlapping cytoplasm segmentation in cervical cytology extended depth of field and volume images," *Computerized Med. Imag. Graph.*, vol. 59, pp. 38–49, Jul. 2017.

[81] A. Kale and S. Aksoy, "Segmentation of cervical cell images," in *Proc. 20th Int. Conf. Pattern Recognit.*, Istanbul, Turkey, Aug. 2010, pp. 2399–2402.

[82] K. P. Win, Y. Kitjaidure, K. Hamamoto, and T. Myo Aung, "Computer-assisted screening for cervical cancer using digital image processing of pap smear images," *Appl. Sci.*, vol. 10, no. 5, p. 1800, Mar. 2020.

[83] I. Muhimmah, R. Kurniawan, and I. Indrayanti, "Overlapping cervical nuclei separation using watershed transformation and elliptical approach in pap smear images," *J. ICT Res. Appl.*, vol. 11, no. 3, p. 213, Dec. 2017.

[84] L. Yang, Y. Lei, Z. Huang, M. Geng, Z. Liu, B. Wang, D. Luo, W. Huang, D. Liang, Z. Pang, and Z. Hu, "An interactive nuclei segmentation framework with Voronoi diagrams and weighted convex difference for cervical cancer pathology images," *Phys. Med. Biol.*, vol. 69, no. 2, Jan. 2024, Art. no. 025021.

[85] M. S. Nosrati and G. Hamarneh, "Segmentation of overlapping cervical cells: A variational method with star-shape prior," in *Proc. IEEE 12th Int. Symp. Biomed. Imag. (ISBI)*, Brooklyn, NY, USA, Apr. 2015, pp. 186–189.

[86] D. Comaniciu and P. Meer, "Mean shift: A robust approach toward feature space analysis," *IEEE Trans. Pattern Anal. Mach. Intell.*, vol. 24, no. 5, pp. 603–619, May 2002.

[87] A. Vedaldi and S. Soatto, "Quick shift and kernel methods for mode seeking," in *Computer Vision—ECCV*. Marseille, France: Springer, Oct. 2008, pp. 705–718.

[88] H. Zhang, H. Zhu, and X. Ling, "Polar coordinate sampling-based segmentation of overlapping cervical cells using attention U-Net and random walk," *Neurocomputing*, vol. 383, pp. 212–223, Mar. 2020.

[89] M. E. Plissiti, C. Nikou, and A. Charchanti, "Automated detection of cell nuclei in pap smear images using morphological reconstruction and clustering," *IEEE Trans. Inf. Technol. Biomed.*, vol. 15, no. 2, pp. 233–241, Mar. 2011.

[90] R. Saha, M. Bajger, and G. Lee, "Spatial shape constrained fuzzy c-means (FCM) clustering for nucleus segmentation in pap smear images," in *Proc. Int. Conf. Digit. Image Comput., Techn. Appl. (DICTA)*, Gold Coast, QLD, Australia, Nov. 2016, pp. 1–8.

[91] S. K. Singh, R. Singh, and A. Goyal, "Semi-automatic segmentation of overlapping cells in pap smear image," in *Proc. 4th Int. Conf. Comput. Sci. (ICCS)*, Jalandhar, India, Aug. 2018, pp. 161–165.

[92] D. Somasundaram, S. Gnanasaravanan, and N. Madian, "Automatic segmentation of nuclei from pap smear cell images: A step toward cervical cancer screening," *Int. J. Imag. Syst. Technol.*, vol. 30, no. 4, pp. 1209–1219, Dec. 2020.
[93] M. Grobe, C. Münzenmayer, H. Kuziela, K. Spinnler, and T. Wittenberg, "A semantic approach to segmentation of overlapping objects," *Methods Inf. Med.*, vol. 43, no. 4, pp. 343–353, 2004.
[94] N. M. Harandi, S. Sadri, N. A. Moghaddam, and R. Amirfattahi, "An automated method for segmentation of epithelial cervical cells in images of ThinPrep," *J. Med. Syst.*, vol. 34, no. 6, pp. 1043–1058, Dec. 2010.
[95] P. Kumar, S. L. Happy, S. Chatterjee, D. Sheet, and A. Routray, "An unsupervised approach for overlapping cervical cell cytoplasm segmentation," in *Proc. IEEE EMBS Conf. Biomed. Eng. Sci. (IECBES)*, Kuala Lumpur, Malaysia, Dec. 2016, pp. 106–109.
[96] H. Nisar, L. Y. Wai, and L. S. Hong, "Segmentation of overlapping cells obtained from pap smear test," in *Proc. IEEE Life Sci. Conf. (LSC)*, Sydney, NSW, Australia, Dec. 2017, pp. 254–257.
[97] M. M. Fatima alias Niraimathi and V. Seenivasagam, "Radial tracing method of cytoplasm segmentation in overlapped cervical cell images," *IETE J. Res.*, vol. 61, no. 4, pp. 402–410, Jul. 2015.
[98] H. A. Phoulady, D. B. Goldgof, L. O. Hall, and P. R. Mouton, "A new approach to detect and segment overlapping cells in multi-layer cervical cell volume images," in *Proc. IEEE 13th Int. Symp. Biomed. Imag. (ISBI)*, Prague, Czech Republic, Apr. 2016, pp. 201–204.
[99] D. Riana, H. Tohir, and A. N. Hidayanto, "Segmentation of overlapping areas on pap smear images with color features using K-means and Otsu methods," in *Proc. 3rd Int. Conf. Informat. Comput. (ICIC)*, Palembang, Indonesia, Oct. 2018, pp. 1–5.
[100] R. Kurniawan, I. Muhimmah, A. Kurniawardhani, and I. Indrayanti, "Segmentation of overlapping cervical cells in normal pap smear images using distance-metric and morphological operation," *CommIT*, vol. 11, no. 1, pp. 25–31, Aug. 2017.
[101] M. Zhao, H. Wang, Y. Han, X. Wang, H.-N. Dai, X. Sun, J. Zhang, and M. Pedersen, "SEENS: Nuclei segmentation in pap smear images with selective edge enhancement," *Future Gener. Comput. Syst.*, vol. 114, pp. 185–194, Jan. 2021.
[102] H. A. Phoulady, D. B. Goldgof, L. O. Hall, and P. R. Mouton, "An approach for overlapping cell segmentation in multi-layer cervical cell, volumes," in *Proc. ISBI*, Mar. 2015, pp. 1–2.
[103] A. Tareef, Y. Song, M.-Z. Lee, D. D. Feng, M. Chen, and W. Cai, "Morphological filtering and hierarchical deformation for partially overlapping cell segmentation," in *Proc. Int. Conf. Digit. Image Comput., Techn. Appl. (DICTA)*, Adelaide, SA, Australia, Nov. 2015, pp. 1–7.
[104] J. Huang, T. Wang, D. Zheng, and Y. He, "Nucleus segmentation of cervical cytology images based on multi-scale fuzzy clustering algorithm," *Bioengineered*, vol. 11, no. 1, pp. 484–501, Jan. 2020.
[105] T. Wang, J. Huang, D. Zheng, and Y. He, "Nucleus segmentation of cervical cytology images based on depth information," *IEEE Access*, vol. 8, pp. 75846–75859, 2020.
[106] R. Saha, M. Bajger, and G. Lee, "Circular shape constrained fuzzy clustering (CiscFC) for nucleus segmentation in pap smear images," *Comput. Biol. Med.*, vol. 85, pp. 13–23, Jun. 2017.
[107] C. Jung, C. Kim, S. W. Chae, and S. Oh, "Unsupervised segmentation of overlapped nuclei using Bayesian classification," *IEEE Trans. Biomed. Eng.*, vol. 57, no. 12, pp. 2825–2832, Dec. 2010.
[108] N. Otsu, "A threshold selection method from gray-level histograms," *Automatica*, vol. 11, nos. 285–296, pp. 23–27, Jun. 1975.
[109] I. T. Hoque, N. Ibtehaz, S. Chakravarty, M. S. Rahman, and M. S. Rahman, "A contour property based approach to segment nuclei in cervical cytology images," *BMC Med. Imag.*, vol. 21, no. 1, pp. 1–12, Jan. 2021.
[110] M. E. Plissiti and C. Nikou, "Overlapping cell nuclei segmentation using a spatially adaptive active physical model," *IEEE Trans. Image Process.*, vol. 21, no. 11, pp. 4568–4580, Nov. 2012.
[111] D. Ushizima, P. H. C. Oliveira, A. G. C. Bianchi, F. N. S. Medeiros, J. F. R. Neto, F. H. D. Araújo, and R. R. V. Silva, "Active contours for overlapping cervical cell segmentation," *Int. J. Biomed. Eng. Technol.*, vol. 35, no. 1, pp. 70–92, 2021.
[112] J. Song, L. Xiao, and Z. Lian, "Contour-seed pairs learning-based framework for simultaneously detecting and segmenting various overlapping cells/nuclei in microscopy images," *IEEE Trans. Image Process.*, vol. 27, no. 12, pp. 5759–5774, Dec. 2018.
[113] D. Riana, A. N. Hidayanto, D. H. Widyantoro, T. L. R. Mengko, and O. Kalsoem, "Segmentation of overlapping cytoplasm and overlapped areas in pap smear images," in *Proc. 8th Int. Conf. Inf., Intell., Syst. Appl. (IISA)*, Larnaca, Cyprus, Aug. 2017, pp. 1–5.
[114] J. Liu, H. Fan, Q. Wang, W. Li, Y. Tang, D. Wang, M. Zhou, and L. Chen, "Local label point correction for edge detection of overlapping cervical cells," *Frontiers Neuroinform.*, vol. 16, May 2022, Art. no. 895290.
[115] A. Bhan, G. Vyas, and S. Mishra, "Supervised segmentation of overlapping cervical pap smear images," in *Proc. Int. Conf. Signal Process. Commun. (ICSC)*, Noida, India, Dec. 2016, pp. 225–228.
[116] Z. Islam and M. A. Haque, "Multi-step level set method for segmentation of overlapping cervical cells," in *Proc. IEEE Int. Conf. Telecommun. Photon. (ICTP)*, Dhaka, Bangladesh, Dec. 2015, pp. 1–5.
[117] T. Wan, S. Xu, C. Sang, Y. Jin, and Z. Qin, "Accurate segmentation of overlapping cells in cervical cytology with deep convolutional neural networks," *Neurocomputing*, vol. 365, pp. 157–170, Nov. 2019.
[118] Y. Huang, H. Zhu, P. Wang, and D. Dong, "Segmentation of overlapping cervical smear cells based on U-Net and improved level set," in *Proc. IEEE Int. Conf. Syst., Man Cybern. (SMC)*, Bari, Italy, Oct. 2019, pp. 3031–3035.
[119] Y. Huang and H. Zhu, "Segmentation of overlapped cervical cells using asymmetric mixture model and shape constraint level set method," *Math. Problems Eng.*, vol. 2020, pp. 1–14, Apr. 2020.
[120] T. Wang, H. Lan, L. Niu, Z. Fan, and G. Yang, "Overlapping cell segmentation of cervical cytology images based on nuclear radial boundary enhancement," *Mobile Inf. Syst.*, vol. 2022, pp. 1–18, Jul. 2022.
[121] K. Roy, D. Bhattacharjee, and M. Nasipuri, "Automated segmentation of cervical cells using MSER algorithm and gradient embedded cost function-based level-set method," in *Proc. ISCMM*, Sikkim, India, Feb. 2019, pp. 91–99.
[122] A. Taneja, P. Ranjan, and A. Ujlayan, "Multi-cell nuclei segmentation in cervical cancer images by integrated feature vectors," *Multimedia Tools Appl.*, vol. 77, pp. 9271–9290, Apr. 2018.
[123] C. Jung and C. Kim, "Segmenting clustered nuclei using H-minima transform-based marker extraction and contour parameterization," *IEEE Trans. Biomed. Eng.*, vol. 57, no. 10, pp. 2600–2604, Oct. 2010.
[124] M. Nosrati and G. Hamarneh, "A variational approach for overlapping cell segmentation," in *Proc. ISBI*, 2014, pp. 1–2.
[125] A. Tareef, Y. Song, W. Cai, H. Huang, Y. Wang, D. Feng, and M. Chen, "Learning shape-driven segmentation based on neural network and sparse reconstruction toward automated cell analysis of cervical smears," in *Proc. ICONIP*, Istanbul, Turkey, Nov. 2015, pp. 390–400.
[126] Y. Song, L. Zhu, B. Lei, B. Sheng, Q. Dou, J. Qin, and K. S. Choi, "Shape mask generator: Learning to refine shape priors for segmenting overlapping cervical cytoplasms," in *Proc. MICCAI*, Lima, Peru, Oct. 2020, pp. 639–649.
[127] A. Tareef, "Adaptive shape prediction model (ASPM) for touched and overlapping cell segmentation in cytology images," *Softw. Impacts*, vol. 17, Sep. 2023, Art. no. 100540.
[128] Y. Song, J. Qin, B. Lei, S. He, and K.-S. Choi, "JOint shape matching for overlapping cytoplasm segmentation in cervical smear images," in *Proc. IEEE 16th Int. Symp. Biomed. Imag. (ISBI)*, Venice, Italy, Apr. 2019, pp. 191–194.
[129] T. P. Deepa and A. N. Rao, "Estimation of a point along overlapping cervical cell nuclei in pap smear image using colour space conversion," *Int. J. Biomed. Eng. Technol.*, vol. 33, no. 1, pp. 77–93, 2020.
[130] J. Fan, Y. Zhang, R. Wang, and S. Li, "A separating algorithm for overlapping cell images," *J. Softw. Eng. Appl.*, vol. 6, no. 4, pp. 179–183, 2013.
[131] Y. Song, A. Zhang, J. Zhou, Y. Luo, Z. Lin, and T. Zhou, "Overlapping cytoplasms segmentation via constrained multi-shape evolution for cervical cancer screening," *Artif. Intell. Med.*, vol. 148, Feb. 2024, Art. no. 102756.
[132] H. Hu, J. Zhang, T. Yang, Q. Hu, Y. Yu, and Q. Huang, "PATrans: Pixel-adaptive transformer for edge segmentation of cervical nuclei on small-scale datasets," *Comput. Biol. Med.*, vol. 168, Jan. 2024, Art. no. 107823.
[133] Y. Zhao, C. Fu, W. Zhang, C. Ye, Z. Wang, and H.-F. Ma, "Automatic segmentation of cervical cells based on star-convex polygons in pap smear images," *Bioengineering*, vol. 10, no. 1, p. 47, Dec. 2022.
[134] J. Ji, W. Zhang, Y. Dong, R. Lin, Y. Geng, and L. Hong, "Automated cervical cell segmentation using deep ensemble learning," *BMC Med. Imag.*, vol. 23, no. 1, p. 137, Sep. 2023.

[135] D. Riana, M. Jamil, S. Hadianti, J. Na'am, H. Sutanto, and R. Sukwadi, "Model of watershed segmentation in deep learning method to improve identification of cervical cancer at overlay cells," *TEM J.*, vol. 12, no. 2, pp. 813–819, May 2023.

[136] W. Zhang, H. Fan, X. Xie, Q. Wang, and Y. Tang, "Mask guidance pyramid network for overlapping cervical cell edge detection," *Appl. Sci.*, vol. 13, no. 13, p. 7526, Jun. 2023.

[137] J. Zhao, Y.-J. He, S.-Q. Zhao, J.-J. Huang, and W.-M. Zuo, "AL-net: Attention learning network based on multi-task learning for cervical nucleus segmentation," *IEEE J. Biomed. Health Informat.*, vol. 26, no. 6, pp. 2693–2702, Jun. 2022.

[138] G. Yang, J. Huang, Y. He, Y. Chen, T. Wang, C. Jin, and P. Sengphachanh, "GCP-net: A gating context-aware pooling network for cervical cell nuclei segmentation," *Mobile Inf. Syst.*, vol. 2022, pp. 1–14, Apr. 2022.

[139] D. Luo, H. Kang, J. Long, J. Zhang, L. Chen, T. Quan, and X. Liu, "Dual supervised sampling networks for real-time segmentation of cervical cell nucleus," *Comput. Struct. Biotechnol. J.*, vol. 20, pp. 4360–4368, Jan. 2022.

[140] G. J. Chowdary and P. Yogarajah, "Nucleus segmentation and classification using residual SE-UNet and feature concatenation approach incervical cytopathology cell images," *Technol. Cancer Res. Treatment*, vol. 22, Feb. 2023, Art. no. 153303382211348.

[141] E. F. Braz and R. D. A. Lotufo, "Nuclei detection using deep learning," in *Proc. Simpósio Brasileiro Telecomunicações Processamento Sinais*, 2017, pp. 1059–1063.

[142] J. Huang, G. Yang, B. Li, Y. He, and Y. Liang, "Segmentation of cervical cell images based on generative adversarial networks," *IEEE Access*, vol. 9, pp. 115415–115428, 2021.

[143] F. H. D. Araújo, R. R. V. Silva, D. M. Ushizima, M. T. Rezende, C. M. Carneiro, A. G. Campos Bianchi, and F. N. S. Medeiros, "Deep learning for cell image segmentation and ranking," *Computerized Med. Imag. Graph.*, vol. 72, pp. 13–21, Mar. 2019.

[144] Y. Song, E.-L. Tan, X. Jiang, J.-Z. Cheng, D. Ni, S. Chen, B. Lei, and T. Wang, "Accurate cervical cell segmentation from overlapping clumps in pap smear images," *IEEE Trans. Med. Imag.*, vol. 36, no. 1, pp. 288–300, Jan. 2017.

[145] Y. Song, L. Zhu, J. Qin, B. Lei, B. Sheng, and K.-S. Choi, "Segmentation of overlapping cytoplasm in cervical smear images via adaptive shape priors extracted from contour fragments," *IEEE Trans. Med. Imag.*, vol. 38, no. 12, pp. 2849–2862, Dec. 2019.

[146] L. Zhu and H. Du, "Instance segmentation of overlapping cervical cells based on boundary tracking," in *Proc. China Autom. Congr. (CAC)*, Oct. 2021, pp. 7600–7604.

[147] K. He, G. Gkioxari, P. Dollár, and R. Girshick, "Mask R-CNN," in *Proc. IEEE Int. Conf. Comput. Vis. (ICCV)*, Oct. 2017, pp. 2980–2988.

[148] J. Chen and B. Zhang, "Segmentation of overlapping cervical cells with mask region convolutional neural network," *Comput. Math. Methods Med.*, vol. 2021, pp. 1–10, Oct. 2021.

[149] Y. Zhou, H. Chen, J. Xu, Q. Dou, and P.-A. Heng, "IRNet: Instance relation network for overlapping cervical cell segmentation," in *Proc. MICCAI*, Shenzhen, China, Oct. 2019, pp. 640–648.

[150] Y. Zhou, H. Chen, H. Lin, and P.-A. Heng, "Deep semi-supervised knowledge distillation for overlapping cervical cell instance segmentation," in *Proc. MICCAI*, Lima, Peru, Oct. 2020, pp. 521–531.

[151] H. Jiang, R. Zhang, Y. Zhou, Y. Wang, and H. Chen, "DoNet: Deep de-overlapping network for cytology instance segmentation," in *Proc. IEEE/CVF Conf. Comput. Vis. Pattern Recognit. (CVPR)*, Vancouver, BC, Canada, Jun. 2023, pp. 15641–15650.

[152] N. Sompawong, J. Mopan, P. Pooprasert, W. Himakhun, K. Suwannarurk, J. Ngamvirojcharoen, T. Vachiramon, and C. Tantibundhit, "Automated pap smear cervical cancer screening using deep learning," in *Proc. 41st Annu. Int. Conf. IEEE Eng. Med. Biol. Soc. (EMBC)*, Berlin, Germany, Jul. 2019, pp. 7044–7048.

[153] X. Li and Q. Li, "Detection and classification of cervical exfoliated cells based on faster R-CNN," in *Proc. IEEE 11th Int. Conf. Adv. INFOCOMM Technol. (ICAIT)*, Jinan, China, Oct. 2019, pp. 52–57.

[154] W. Zhao and X. Zhou, "Bi-polar mask for joint cell and nuclei instance segmentation," in *Proc. IEEE Int. Conf. Image Process. (ICIP)*, Bordeaux, France, Oct. 2022, pp. 3421–3425.

[155] I. Goodfellow, J. Pouget-Abadie, M. Mirza, B. Xu, D. Warde-Farley, S. Ozair, A. Courville, and Y. Bengio, "Generative adversarial networks," *Commun. ACM*, vol. 63, no. 11, pp. 139–144, Oct. 2020.

[156] X. Hao, L. Pei, W. Li, Y. Liu, and H. Shen, "An improved cervical cell segmentation method based on deep convolutional network," *Math. Problems Eng.*, vol. 2022, pp. 1–13, Mar. 2022.

E CHEN received the Diploma degree in applied electronic technology from Hubei University of Technology, China, in 2010, and the M.S. degree in software engineering from Wuhan Textile University, in 2016. He is currently pursuing the Ph.D. degree with the Faculty of Engineering, Universiti Malaya. His research interests include machine learning, deep learning, and cervical cancer detection.

HUA-NONG TING received the B.E. degree in medical electronics and the master's and Ph.D. degrees in electrical engineering from the University of Technology Malaysia, Malaysia, in 2000, 2002, and 2007, respectively. He is currently an Associate Professor with the Department of Biomedical Engineering, Faculty of Engineering, Universiti Malaya. His current research interests include speech analysis and recognition, artificial neural networks, deep learning, and dielectric measurement. He is a member of the Institute of Engineering and Technology (IET), a Chartered Engineer of the Engineering Council, U.K., and a Professional Engineer (Ir) with the Board of Engineers Malaysia.

JOON HUANG CHUAH (Senior Member, IEEE) received the B.Eng. degree (Hons.) from Universiti Teknologi Malaysia, the M.Eng. degree from the National University of Singapore, and the M.Phil. and Ph.D. degrees from the University of Cambridge. He is currently a Professor and the President and CEO of Southern University College, Malaysia. He is also the Head of the VIP Research Group, Department of Electrical Engineering, Faculty of Engineering, Universiti Malaya, Malaysia. His main research interests include image processing, computational intelligence, IC design, and scanning electron microscopy. He is a fellow and the Vice President of the Institution of Engineers, Malaysia (IEM). He was the Honorary Treasurer of the IEEE Computational Intelligence Society (CIS) Malaysia Chapter and the Honorary Secretary of the IEEE Council on RFID Malaysia Chapter. He is the Chairperson of the Institution of Engineering and Technology (IET) Malaysia Network. He is also a Chartered Engineer registered under the Engineering Council, U.K., and a Professional Engineer registered under the Board of Engineers, Malaysia.

JUN ZHAO (Member, IEEE) received the Ph.D. degree from the Department of Biomedical Engineering, Shanghai Jiao Tong University, Shanghai, China, in 2006. He was a Visiting Scholar with the University of Iowa, USA, from 2006 to 2007. He is currently a tenured Professor with the School of Biomedical Engineering, Shanghai Jiao Tong University. His research interests include biomedical imaging, medical image processing, computer-aided detection, and medical applications of synchrotron radiation.